ELSEVIER

Journal of Nuclear Materials 303 (2002) 1–28

journal of nuclear materials

www.elsevier.com/locate/jnucmat

Progress in the thermodynamic modelling of the O–U binary system

P.-Y. Chevalier *, E. Fischer, B. Cheynet

Thermodata, INPG-CNRS (UMS THERMA), BP 66, F-38402 Saint Martin d'Hères cedex, France

Received 27 July 2001; accepted 18 February 2002

Abstract

The fuel of civil nuclear plants, UO_2, melts at 3120 K. During an hypothetical severe accident, urania, submitted to high temperatures and various oxygen potentials, presents a wide non-stoichiometry range: the melting temperature of $UO_{2\pm x}$, related to oxygen potential, decreases in all cases. In this scenario, urania could react with other materials, firstly zircaloy, and the melting temperature of (U, Zr)$O_{2\pm x}$ still decreases. That is why the critical assessment of the O–U binary system including the non-stoichiometry range of urania, is a major step to a correct thermodynamic modelling of multicomponent systems for nuclear safety. The very numerous experimental information has been compiled and analysed. The associate model was used for the liquid phase, and a sublattice model for $UO_{2\pm x}$; U_4O_{9-y}, U_3O_8 and UO_3 were treated as stoichiometric. Phase diagram and thermodynamic properties have been calculated from the optimised Gibbs energy parameters. The calculated consistency with the experimental ones is quite satisfactory. © 2002 Published by Elsevier Science B.V.

1. Introduction

The thermodynamic modelling of the O–U system is of first importance in the development of a nuclear thermodynamic database. In the unlikely event of a severe accident, all materials of a nuclear plant may interact thermochemically: fuel (UO_2), zircaloy (Zr), steel structures (Fe, Cr, Ni), control rods (Ag, Cd, In) or boron carbide (B, C), fission products (Ba, La, Ru, Sr), concrete (Al_2O_3, CaO, FeO, Fe_2O_3, MgO, SiO_2), water and air (H, O). This inventory allows one to identify the main components involved. Then, the thermodynamic modelling of the selected multicomponent system is based on the critical assessment of all the binary and the most important higher-order subsystems (metallic, oxide, metal–oxygen). The O–U binary system is the first of all.

In the first step of an eventual severe accident, the fuel rods may melt and interact with other materials, leading to the core degradation. At high temperature, UO_2 reacts with the metallic zircaloy and is partially disintegrated. A ceramic solid solution (U, Zr)$O_{2\pm x}$ in equilibrium with a ternary (O–U–Zr) liquid phase is formed. The thermochemical properties of this system (liquidus, solidus, phase proportions) are needed to be linked to more global thermohydraulics safety codes dedicated to the in-vessel core degradation. Consequently, a precise knowledge of the ternary metal–oxygen O–U–Zr system is needed and that is why its thermodynamic modelling has been undertaken in a previous work by Chevalier and Fischer [1], from a critical assessment of all the available experimental information, equilibrium phase diagram and thermodynamic properties.

Unfortunately, at that time, the experimental information provided by different sources was not consistent in some specific fields. The main identified incoherencies concerned the limit of solubility of oxygen in U or U–Zr alloys and the extension of the liquid miscibility gap in the O–U binary and O–U–Zr ternary systems.

Owing to all the encountered experimental inconsistencies on the liquidus shape from 2073 K to very high

* Corresponding author.

0022-3115/02/$ - see front matter © 2002 Published by Elsevier Science B.V.
PII: S0022-3115(02)00813-9

temperatures (above 3000 K), two different set of Gibbs energy parameters were proposed in our previous work [1] for the O–U and O–U–Zr ternary system. The first one corresponded to a small solubility of oxygen in U or U–Zr liquid alloys and a large miscibility gap, the second one to a larger solubility and a smaller miscibility gap. The two versions differed only on O–U and O–U–Zr excess interaction parameters, but did not succeed to reproduce simultaneously all the experimental points.

From this analysis, it appeared obviously that future efforts should be made on the interpretation of the existing experiments in terms of thermodynamic equilibrium and that there was a lack of experimental information at high temperature.

The O–U binary system is certainly one of the most complex systems of the periodic table. The experimental information concerning phase diagram and thermodynamic properties is very numerous and their compilation has been undertaken for many years.

Today, new experiments are available on the miscibility gap in the liquid state both in the O–U and O–U–Zr systems and the experimental methods for oxygen solubility measurements have been carefully re-analysed to discard non-equilibrium measurements. Moreover, the set of experimental data has been completed: especially, very numerous oxygen potentials of $UO_{2\pm x}$ at various temperatures and phase diagram data in the hyper-stoichiometric range ($UO_{2+x} + U_4O_{9-y}$) and ($U_4O_{9-y} + U_3O_{8-z}$) at low temperature have been taken into account; the heat capacity and heat content of stoichiometric compounds was also compiled in order to include second-order anomalies not previously described.

At last, the influence of the choice of the defects used in the sublattice model for $UO_{2\pm x}$ was analysed, because it may affect the quality of the self-consistency of thermodynamic properties.

All these points argue that a new critical assessment (phase diagram and thermodynamic properties) and thermodynamic modelling of the O–U binary system was quite necessary for building a high quality and reliable nuclear thermodynamic database.

2. Presentation of the O–U phase diagram

The phase diagram of the O–U binary system has been successively reported in a compilation work by Levin et al. [2] and Roth et al. [3]. The condensed solutions and stoichiometric substances, with the symbols currently used in this work, are the following: liquid phase, L; $UO_{2\pm x}$ solid solution, fcc_C1, O_2U_1(S); U_4O_{9-y}, O_9U_4(S); U_3O_{8-z}, O_8U_3(S); UO_3, O_3U_1(S); $U_5O_{13\pm x}$, $O_{13}U_5$(S); U_8O_{21}, $O_{21}U_8$(S); $UO_{2.61}$, $O_{2.61}U_1$(S); α-U, U_1(ort_A20); β-U, U_1(tet); γ-U, U_1(bcc_A2).

Pure urania UO_2 melts at 3120 K. Urania presents a large non-stoichiometric range, indicated by the formula $UO_{2\pm x}$. The hypo-stoichiometric range of UO_{2-x} is well known, while the hyper-stoichiometric range of UO_{2+x} is well determined only below 1900 K.

In the hypo-stoichiometric range (UO_{2-x}), the liquidus decreases down to the monotectic reaction L_1 (oxide-rich) $\Longleftrightarrow UO_{2-x} + L_2$ (uranium-rich), at about 2700 K. Above this temperature, a liquid miscibility gap $L_1 + L_2$ and a diphasic region $UO_{2-x} + L_1$ exist. Below this temperature, a diphasic region $UO_{2-x} + L_2$ exists, and the solubility of oxygen in L_2 decreases down to the eutectic reaction $L_2 \Longleftrightarrow UO_{2-x} + \gamma$-U, deported on the uranium-rich side, not far from the uranium melting point (1408 K). Below this temperature, only the uranium transitions occur at 1049 K (β-U $\Longleftrightarrow$ γ-U)and 942 K (α-U $\Longleftrightarrow$ β-U). The solubility of oxygen in L_2 was subject to discussion, as the width of the liquid miscibility gap.

In the hyper-stoichiometric range (UO_{2+x}), the liquidus decreases down to the invariant reaction L_1 (oxide-rich) $\Longleftrightarrow UO_{2+x} +$ Gas. The complex gas phase is composed of different species, O_1(G), O_2(G), O_3(G), U_1(G), U_1O_1(G), U_1O_2(G), U_1O_3(G), and the temperature of this invariant reaction depends on total pressure. This temperature is not experimentally determined under one atmosphere, because the liquidus was measured in sealed containers. Above this temperature, two diphasic regions $UO_{2+x} + L_1$ and $L_1 +$ G exist. Below this temperature, the diphasic domain $UO_{2+x} +$ G exists down to the invariant reaction $G + UO_{2+x} \Longleftrightarrow U_3O_{8-z}$, estimated around 2000 K in the compilations. At temperature below 1400 K, other intermediate phases were identified. U_4O_{9-y} is stable up to the invariant reaction $UO_{2+x} + U_3O_{8-z} \Longleftrightarrow U_4O_{9-y}$; UO_3 is stable up to the invariant reaction $G + U_3O_{8-z} \Longleftrightarrow UO_3$. Thus, the diphasic domains $G + UO_3$, $UO_3 + U_3O_{8-z}$, $U_3O_{8-z} + U_4O_{9-y}$, $U_4O_{9-y} + UO_{2+x}$, exist at low temperature; the diphasic domains $G + U_3O_{8-z}$ and $U_3O_{8-z} + UO_{2+x}$ exist between 1400 and 2000 K approximately. The arrangement of neighbour compounds designated as $UO_{2.61}$, U_8O_{21} (O/U = 2.625), U_5O_{13} (O/U = 2.6) and U_3O_8 (O/U = 2.667) is not clear. It exists probably two intermediate compounds with a limited non-stoichiometric range and designated by U_3O_{8-z} ($2.66 < O/U < 2.667$) and $U_8O_{21} \pm x$ ($2.61 < O/U < 2.66$). The very limited non-stoichiometric range of U_4O_{9-y} is better known.

3. Experimental information

In the following, T is the temperature in Kelvin, x(U) the atomic fraction of uranium in the O–U system, O/U the oxygen/uranium atomic ratio, L the liquidus or the liquid, and S the solidus.

The compilation of available experimental information has been previously undertaken [1]. It has been completed in this work by new available data and

missing data in the hyper-stoichiometric field at temperatures below 1900 K.

3.1. Phase diagram

3.1.1. Solid–liquid equilibria

The solidus ($UO_{2-x}/UO_{2-x}+L_2$), i.e. the hypo-stoichiometric boundary of urania, has been determined by Bates [4] by micrographic observations: the composition of UO_{2-x}, $x^S(U)$, varied from 0.3416 at 2073 K to 0.3597 at 2673 K.

Martin and Edwards [5] have established the existence of a liquid miscibility gap of substantial width by the metallographic examination of arc-melted alloys in a wide range of composition. The monotectic reaction has been established at 2773 ± 30 K and $x^{L_1}(U) = 0.4348$, from experiments in which uranium was heated in uranium dioxide crucibles. The solidus and liquidus data below 2773 K were obtained from equilibration of uranium melts with uranium dioxide in a purified helium atmosphere, then quenched to room temperature. The liquidus data ($L_2/L_2 + UO_{2-x}$) were provided by the analyses of the uranium ingot products: the composition of liquid, $x^{L_2}(U)$, varied from 0.9974 at 2181 K to 0.9763 at 2683 K. The solidus data ($UO_{2-x}/UO_{2-x}+L_2$) were provided by the analyses of uranium oxide growths formed between the uranium melts and the crucibles: the composition of UO_{2-x}, $x^S(U)$, varied from 0.3373 at 1873 K to 0.3777 at 2745 K.

The liquidus ($L_2/(L_2 + UO_{2-x})$) of the uranium–uranium dioxide system has been determined firstly by Blum et al. [6], by the saturation method: the composition of liquid, $x^{L_2}(U)$, varied from 0.767 at 1803 K to 0.457 at 2553 K.

The liquidus has been re-determined later on with the same method and the solidus by analysis of the samples in equilibrium with the liquid at each temperature by Guinet et al. [7]. Compositions were established by micrographic and chemical analysis. The phase diagram is of eutectic type (1403 K) deported on the uranium-rich side, and shows a narrow liquid miscibility gap at high temperature. The monotectic was located at 2743 ± 30 K and $x^{L_1}(U) = 0.4587$. The compositions of the solid, $x^{UO_{2-x}}(U) = 0.3846$, and liquid, $x^{L_2}(U) = 0.516$, were extrapolated from the liquidus and solidus data obtained at lower temperature. The composition of the solid at the monotectic temperature was also reported from micrographic analysis as $x^S(U) = 0.3855$; 0.3828; 0.3794. The liquidus composition, $x^{L_2}(U)$, varied from 0.893 at 1803 K to 0.6024 at 2573 K; the solidus ($UO_{2-x}/UO_{2-x}+L_2$) composition, $x^S(U)$, varied from 0.3521 at 2223 K to 0.3690 at 2573 K.

The melting temperature for hypo-stoichiometric UO_{2-x} ($L_1/(L_1 + UO_{2-x})$) has been determined by Bates [8] in an electric furnace with purified inert atmospheres by microscopy and optical brightness pyrometry. It varied from 3063 ± 17 K for $x(U) = 0.33311$ to 2806 ± 31 K for $x(U) = 0.3723$.

Both solidus and liquidus temperatures on the UO_2-rich side have been measured (± 70 K) by Bannister [9]. The monotectic was located at 2693 K and $x^S(U) = 0.382$, the melting point of UO_2 at 3133 K, (although another value taken from literature, 3078 ± 15 K, was also reported in the original paper). The liquidus ($L_1/(L_1 + UO_{2-x})$) temperature varied from 2993 K for $x^{L_1}(U) = 0.356$ at 2693 K for $x^{L_1}(U) = 0.396$. The solidus temperature, ($UO_{2-x}/UO_{2-x}+L_1$) varied from 2963 K for $x^S(U) = 0.351$ to 2693 K for $x^S(U) = 0.384$.

The phase diagram (temperature–pressure composition) in the UO_2–U composition and 1600–2500 K temperature ranges has been investigated by Ackermann et al. [10]. The solidus composition ($UO_{2-x}/UO_{2-x}+L_2$) was determined by an isopiestic method and varied from $x^S(U) = 0.3378$ at 1873 K to $x^S(U) = 0.3716$ at 2523 K.

The solidus in agreement with the phase boundary data of Martin and Edwards [5] has been reported on a $\log P(O)$–T–O/U diagram by Tetenbaum and Hunt [11,12]. The solidus composition ($UO_{2-x}/UO_{2-x}+L_2$) varied from $x^S(U) = 0.3424$ at 2080 K to $x^S(U) = 0.3805$ at 2705 K.

Solidus and liquidus temperatures for urania have been determined by Latta and Fryxell [13] by a thermal arrest technique, using samples sealed in tungsten or rhenium. The melting point of UO_2 was given as 3138 K and the monotectic determined as 2698 K, $x^S(U) = 0.3745$, $x^{L_1}(U) = 0.4065$. The absolute accuracy of the temperature measurements (± 15 K) was verified by melting Ta, Mo and Al_2O_3 (sapphire) as standards. Solidus and liquidus temperatures decreased down to 2837 and 3031 K for $x(U) = 0.3096$ in the hyper-stoichiometric range and down to 2701 and 2771 K for $x(U) = 0.4$ in the hypo-stoichiometric range.

The solubility of oxygen in liquid uranium and the composition of the lower phase boundary of uranium dioxide at 1950 K has been determined as $x^{L_2}(U) = 0.9438$ and $x^S(U) = 0.33908$ by Garg and Ackermann [14], using a simple method, developed by Ackermann and Rauh [15] and Garg and Ackermann [16], which does not involve post-experimental evaluation of the quenched sample.

New data on the liquid miscibility gap in the O–U binary system and the O–U–Zr ternary system, have been recently reported by Gueneau et al. [17] and allowed to determine one tie line in each of these two systems. The following results were obtained for O–U at 3090 ± 100 K, $x^{L_1}(U) = 0.45 \pm 0.02$, $x^{L_2}(U) = 0.98 \pm 0.02$.

The experimental compositions and temperatures of solid–liquid equilibria measured by the different authors have been reported in Table 1 ($L_1 \Longleftrightarrow UO_{2-x} + L_2$), Table 2 ($UO_{2-x}/UO_{2-x}+L_2$), Table 3 ($L_2/L_2 + UO_{2-x}$) and Table 4 ($UO_{2\pm x}/UO_{2\pm x} + L_1$, $L_1/L_1 + UO_{2\pm x}$).

Table 1
Experimental and calculated monotectic reaction $L_1 \Longleftrightarrow UO_{2-x} + L_2$

T (K)	x^{L_1}(U)	x^{S}(U)	x^{L_2}(U)	Reference
2773 ± 30	0.435	0.378	0.976	[5]
2743 ± 30	0.459	0.385	0.516	[7]
2698 ± 15	0.406	0.375	0.965	[13]
2692	0.419	0.374	0.960	Calc.

3.1.2. Solid–solid equilibria

The oxygen dissociation pressures over the uranium oxides ($2.0 < O/U < 2.62$, $1223 < T < 1423$ K) have been measured by Blackburn [18] by the Knudsen effusion method: three stable uranium oxides were identified: UO_{2+x}, in which x increases with temperature, $U_4O_{9\pm y}$ with a narrow homogeneity range, and $U_5O_{13+z}(UO_{2.61})$. A partial phase diagram was constructed and thermodynamic values were derived.

The $UO_{2+x} + U_4O_{9-y}$ phase diagram ($2.0 < O/U < 2.2$, $630 < T < 1215$ K) has been established by Schaner [19] by using metallographic techniques.

The equilibrium oxygen pressures ($2.0 < O/U < 2.30$, $1273 < T < 1723$ K) have been directly determined by Roberts and Walter [20] by tensimetric experiments. An invariant reaction $UO_{2+x} + UO_{2.61} \Longleftrightarrow U_4O_{9-y}$ was

Table 2
Experimental and calculated solidus ($UO_{2-x}/UO_{2-x} + L_2$), i.e. hypo-stoichiometric urania boundary below the monotectic temperature

T^S (K)	$x^{S,exp}$(U)	$x^{S,calc}$(U)	T^S (K)	x^S(U)	$x^{S,calc}$(U)
	[4]			[10]	
2073	0.3416	0.3429	1873	0.3378	0.3382
2273	0.3475	0.3503	2023	0.3412	0.3415
2473	0.3520	0.3604	2102	0.3423	0.3438
2673	0.3597	0.3726	2192	0.3471	0.3469
	[5]		2248	0.3483	0.3492
1873	0.3373	0.3382	2346	0.3532	0.3536
2093	0.3420	0.3435	2423	0.3598	0.3576
2196	0.3472	0.3471	2486	0.3634	0.3611
2268	0.3493	0.3500	2508	0.3663	0.3624
2373	0.3521	0.3550	2523	0.3716	0.3633
2483	0.3610	0.3609		[11,12]	
2526	0.3662	0.3635	2080	0.3424	0.3431
2599	0.3742	0.3679	2185	0.3464	0.3467
2699	0.3779		2290	0.3506	0.3510
2745	0.3777		2390	0.3560	0.3559
	[7]		2495	0.3619	0.3616
2223	0.3521	0.3482	2600	0.3699	0.3680
2443	0.3636	0.3587	2705	0.3805	
2493	0.3650	0.3615		[14]	
2573	0.3690	0.3663	1950	0.3391	0.3397
2743	0.3846				

Table 3
Experimental and calculated liquidus ($L_2/L_2 + UO_{2-x}$), i.e. uranium-rich liquid boundary below the monotectic temperature

T^{L_2} (K)	$x^{L_2,exp}$(U)	$x^{L_2,calc}$(U)	T^{L_2} (K)	$x^{L_2,exp}$(U)	$x^{L_2,calc}$(U)
	[5]			[7]	
2181	0.9974	0.9935	1803	0.8930	0.9991
2256	0.9949	0.9912	2003	0.8621	0.9972
2258	0.9924	0.9911	2133	0.7911	0.9948
2499	0.9824	0.9785	2223	0.7599	0.9923
2581	0.9874	0.9718	2293	0.7300	0.9898
2683	0.9536	0.9609	2433	0.7100	0.9829
2683	0.9763	0.9609	2503	0.6580	0.9782
	[6]		2573	0.6024	0.9725
1803	0.767	0.9991		[14]	
1953	0.685	0.9978	1950	0.9438	0.9979
2233	0.561	0.9920			
2553	0.457	0.9743			

Table 4
Experimental and calculated liquidus ($L_1/L_1 + UO_{2\pm x}$) and solidus ($UO_{2\pm x}/UO_{2\pm x} + L_1$) above the monotectic temperature in the oxide-rich field

T^{L_1} (K)	$x^{L_1,exp}(U)$	$x^{L_1,calc}(U)$	T^{S} (K)	$x^{S,exp}(U)$	$x^{S,calc}(U)$
	[8]				
2806	0.37230	0.3923			
2841	0.36860	0.3857			
2921	0.36563	0.3718			
2937	0.35997	0.3691			
2876	0.35971	0.3795			
2900	0.35817	0.3753			
2971	0.35791	0.3636			
2954	0.35676	0.3664			
2994	0.35423	0.3600			
2974	0.35199	0.3632			
3019	0.34868	0.3560			
2989	0.34831	0.3608			
2976	0.34746	0.3628			
3017	0.34614	0.3563			
3008	0.34282	0.3578			
3065	0.34223	0.3485			
3077	0.33322	0.3464			
3063	0.33311	0.3488			
	[9]			[9]	
2693	0.396	0.4184	2693	0.384	0.3739
2753	0.387	0.4033	2753	0.372	0.3710
2798	0.384	0.3939	2823	0.364	0.3679
2933	0.364	0.3698	2893	0.356	0.3550
2993	0.356	0.3601	2963	0.351	0.3487
	[13]			[13]	
3031	0.3096	0.3119	2837	0.3096	0.3126
3013	0.3096	0.3087	2851	0.3096	0.3131
3045	0.3141	0.3145	2878	0.3141	0.3140
3078	0.3195	0.3215	2940	0.3195	0.3163
3071	0.3205	0.3199	2907	0.3205	0.3150
3088	0.3231	0.3239	3003	0.3231	0.3195
3090	0.3231	0.3244	3001	0.3231	0.3193
3109	0.3270	0.3299	3067	0.3270	0.3245
3136	0.3309		3085	0.3309	0.3267
3125	0.3312		3109	0.3312	0.3309
3138	0.3336		3118	0.3336	0.3359
3135	0.3337		3120	0.3337	0.3356
3133	0.3337		3107	0.3337	0.3372
3133	0.3341		3105	0.3341	0.3375
3133	0.3356		3106	0.3356	0.3373
3130	0.3383		3076	0.3383	0.3404
3118	0.3398	0.3375	3069	0.3398	0.3411
3113	0.3425	0.3390	3043	0.3425	0.3437
3105	0.3460	0.3409	3002	0.3460	0.3478
3083	0.3501	0.3453	2970	0.3501	0.3511
3033	0.3560	0.3538	2888	0.3560	0.3597
3033	0.3568	0.3538	2893	0.3568	0.3592
3031	0.3580	0.3541	2874	0.3580	0.3611
2983	0.3636	0.3617	2818	0.3636	0.3662
3013	0.3584	0.3570	2863	0.3584	0.3622
2968	0.3655	0.3641	2786	0.3655	0.3688
2923	0.3757	0.3715	2686	0.3757	0.3735
2857	0.3846	0.3828	2696	0.3846	0.3738
2783	0.3912	0.3969	2708	0.3912	0.3733
2771	0.4000	0.3994	2701	0.4000	0.3736

Table 5
Experimental and calculated compositions and temperatures of $UO_{2+x}(\Phi1) + U_4O_{9-y}(\Phi2)$

T (K)	$x^{\Phi1,exp}(U)$	$x^{\Phi2,exp}(U)$	$x^{\Phi1,calc}(U)$	T (K)	$x^{\Phi1,exp}(U)$	$x^{\Phi2,exp}(U)$	$x^{\Phi1,calc}(U)$
	[18]				[28]		
1353	0.30979	0.30779	0.3094	853	0.3204		0.3198
1331	0.31094	0.30874	0.3099	831	0.3202		0.3206
1309	0.31211	0.30883	0.3103	856	0.3193		0.3197
1285	0.31279	0.30912	0.3107	883	0.3187		0.3198
1263	0.31309	0.30941	0.3111	890	0.3184		0.3187
1239		0.30941	0.3115	935	0.3168		0.3175
	[19]			1071	0.3148		0.3145
630	0.3324		0.3320	1143	0.3135		0.3132
689	0.3310		0.3299	1043	0.3148		0.3151
720	0.3287		0.3272	1134	0.3135		0.3134
750	0.3270		0.3246	1238	0.3125		0.3115
769	0.3253		0.3234		[29]		
767	0.3229		0.3235	673	0.3289		0.3307
838	0.3198		0.3203	738	0.3258		0.3256
1124	0.3152		0.3135	756	0.3236		0.3242
1152	0.3145		0.3130	771	0.3225		0.3233
1215	0.3132		0.3119	810	0.3186		0.3214
	[20]			888	0.3178		0.3188
1324	0.31192		0.3100	983	0.3171		0.3164
1341		0.30874	0.3097	1014	0.3165		0.3157
1344	0.31104		0.3096	1069	0.3155		0.3146
1350	0.31046		0.3095	1207	0.3138		0.3121
1377	0.30960		0.3089		[30]		
1388		0.30817	0.3086	298		0.30979	0.3333
1392	0.30874	0.30792	0.3084		[32]		
1396	0.30826		0.3083	1323	0.31124	0.3093	0.3100
	[21]				[34]		
798	0.32237		0.3219	673	0.3311		0.3307
918	0.31857		0.3179	696	0.3300		0.3294
928	0.31817		0.3177	710	0.3289		0.3282
1233	0.31466		0.3116	723	0.3279		0.3269
1248	0.31447		0.3113	733	0.3268		0.3260
1313	0.31309		0.3102	741	0.3257		0.3253
1328	0.31182		0.3099	746	0.3247		0.3249
1348	0.31133		0.3095	754	0.3236		0.3243
1373	0.30969		0.3090	765	0.3226		0.3236
1368	0.30921		0.3091	782	0.3215		0.3227
	[24]			800	0.3205		0.3218
1355	0.3107	0.30921	0.3094	838	0.3195		0.3203
1370	0.3104	0.30899	0.3091	890	0.3185		0.3187
1394	0.3092	0.30880	0.3084	937	0.3175		0.3175
1401	0.3086		0.3080	986	0.3165		0.3163
	[25]			1047	0.3155		0.3150
298		0.30912	0.3333	1120	0.3145		0.3136
1373		0.30912	0.3090	1189	0.3135		0.3124
				1243	0.3125		0.3114
	[26]			1298	0.3115		0.3105
293		0.3096, –, 0.31046		1341	0.3106		0.3097
623		0.3101, 0.3106, 0.3106		1379	0.3096		0.3088
723		0.3109, 0.31147, –		1403	0.3086		0.3080
823		–, 0.3114, 0.31017			[35]		
923		0.31056, 0.3101, 0.31046		1073	0.31646		0.3145
1073		0.3096, 0.30998, 0.30998		1173	0.31358		0.3127
	[28]			1273	0.31066		0.3109
673	0.3322		0.3307	1373	0.30874		0.3090
695	0.3316		0.3295	1423	0.30817		0.3080

Table 5 (*continued*)

T (K)	$x^{\Phi1,\exp}(U)$	$x^{\Phi2,\exp}(U)$	$x^{\Phi1,\mathrm{calc}}(U)$	T (K)	$x^{\Phi1,\exp}(U)$	$x^{\Phi2,\exp}(U)$	$x^{\Phi1,\mathrm{calc}}(U)$
689	0.3308		0.3299	1473	0.30788		0.3080
726	0.3281		0.3266				
741	0.3270		0.3253				
745	0.3270		0.3250				
768	0.3243		0.3235				
805	0.3242		0.3216				
809	0.3221		0.3214				
827	0.3210		0.3207				

Table 6
Experimental and calculated compositions and temperatures of $UO_{2+x}(\Phi1) + U_8O_{21\pm x}(\Phi2)$

T (K)	$x^{\Phi1,\exp}(U)$	$x^{\Phi2,\exp}(U)$	$x^{\Phi2,\mathrm{calc}}(U)$	T (K)	$x^{\Phi1,\exp}(U)$	$x^{\Phi2,\exp}(U)$	$x^{\Phi1,\mathrm{calc}}(U)$
	[20]				[23]		
1396	0.30826	0.27701	0.3083	1373		0.27685	0.3080
1423	0.30817	0.27701	0.3080	1473		0.27685	0.3080
1511	0.30788	0.27701	0.3080	1573	0.30817	0.27685	0.3080
1550	0.30750	0.27701	0.3080	1673	0.30769		0.3081
1626	0.30760	0.27701	0.3080	1673	0.30722		0.3081
1666	0.30684	0.27701	0.3081		[24]		
	[22]			1401		0.27639	0.3080
1473	0.30864	0.27701	0.3080	1410	0.30861		0.3080
1566	0.30779	0.27701	0.3080	1415	0.30859		0.3080
1618	0.30731	0.27701	0.3080	1420	0.30873		0.3080
1660	0.30684	0.27701	0.3080	1439		0.27619	0.3080
1779	0.30600	0.27701	0.3081	1450	0.30848		0.3080
1911	0.30562	0.27701	0.3083	1460	0.30858		0.3080
					[35]		
				1423	0.30817		0.3080
				1473	0.30788		0.3080

Table 7
Experimental compositions and temperatures of $U_4O_{9\pm y}(\Phi1) + U_8O_{21\pm x}(\Phi2)$ measured by the different authors

T (K)	$x^{\Phi1}(U)$	$x^{\Phi2}(U)$	Reference	T (K)	$x^{\Phi1}(U)$	$x^{\Phi2}(U)$	Reference
1399		0.27655	[18]	1373	0.30864		[25]
1376	0.30628	0.27723		298	0.30817		
1353	0.30544						
1331	0.30497	0.27739		298	0.30769		[30]
1309	0.30675						
1285	0.30647			1323	0.30845		[32]
1263	0.30731	0.27708					
1239	0.30544			998		0.27648	[33]
1215		0.27701		1159		0.27649	
1125		0.27724		1243		0.27656	
				1371		0.27668	

found at 1396 ± 5 K. The non-stoichiometry domain of U_4O_9 was below $O/U = 2.25$. The relevant parts of the phase diagram were constructed and the thermodynamic properties ΔG, ΔH and ΔS for the formation of all intermediate phases intermediate between $UO_{2.00}$ and U_3O_8 were given.

The UO_{2+x} phase boundary has been determined by Aronson et al. [21] with U_4O_{9-y} by electrical conductivity and thermoelectric power measurements (773–1423 K).

The phase diagram (1500–2000 K) has been established by Anthony et al. [22] by quenching uranium

Table 8
Experimental compositions and temperatures of $U_8O_{21\pm x}(\Phi1) + U_3O_{8-z}(\Phi2)$ measured by the different authors

T (K)	$x^{\Phi1}$(U)	$x^{\Phi2}$(U)	Reference	T (K)	$x^{\Phi1}$(U)	$x^{\Phi2}$(U)	Reference
1024		0.27283	[31]	844	0.27353	0.27273	[33]
1125	0.27377			998	0.27362	0.27276	
1134		0.27281		1159	0.27357	0.27279	
1176	0.27382			1243	0.27355	0.27284	
1254		0.27264					

Table 9
Experimental and calculated temperature of the peritectoid reaction $UO_{2+x} + U_3O_{8-z} \Longleftrightarrow U_4O_{9-y}$

T (K)	Reference
1399.15	[18]
1396.15	[20]
1398.15	[25]
1401.65	[30]
1400.00	Calc.

oxide samples held at a fixed temperature and known P_{O_2}. The O/U ratio was measured by means of a thermobalance and phases determined by X-ray analysis.

The non-stoichiometry in the phases UO_{2+x} and U_3O_{8-z} has been determined versus P_{O_2} by use of a thermobalance (1173–1773 K) by Hagemark and Broli [23].

The limits of the phases ($2.19 < O/U < 2.63$, 1353–1473 K) have been obtained by Kotlar et al. [24] by the

Table 10
Experimental and calculated thermodynamic properties of formation of stoichiometric compounds

	$\Delta H^0_{f(298.15\,K)}$ kJ mol^{-1}	Reference	$S^0_{f(298.15\,K)}$ J mol^{-1} K^{-1}	Reference
UO_2				
	-1084.9112 ± 0.8368	[41]		
	-1083.6560 ± 2.5104	[44]		
	-1084.9112 ± 0.8368	[36]	77.02744	[36]
	−1084.9112	[37]	77.02744	[37]
	−1084.9112	(Calc.)	77.02744	(Calc.)
U_4O_9				
	-4510.7704 ± 15.0624	[43]	335.93336 ± 0.33472	[50]
	-4510.3520 ± 16.7360	[44]	349.53136	[53]
	−4490.6872	[47]	333.68237	[54]
	−4550.5184	[48]		
	-4512.0000 ± 7	[37]	334.10000 ± 0.7	[37]
	−4512.0000	(Calc.)	334.10000	(Calc.)
U_3O_8				
	−3536.3168	[38]		
	-3571.0440 ± 6.6944	[40]		
	-3574.8096 ± 2.5104	[41]		
	-3583.5960 ± 12.9704	[42]		
	-3573.5544 ± 8.368	[44]		
	−3599.9136	[48]		
	-3574.8000 ± 2.5	[37]	282.55000 ± 0.5	[37]
	−3573.5546	(Calc.)	282.4206	(Calc.)
UO_3				
	−1271.5176	[38]		
	−1224.5173	[39]		
	-1222.9832 ± 5.8576	[43]		
	-1225.9120 ± 8.368	[44]		
	-1228.0040 ± 4.184	[45]	85.102	[45]
	-1237.6272 ± 1.8828	[46]	98.617 ± 0.25	[61]
	−1231.7696	[48]	96.11	[62]
	-1224.1000 ± 2.6	[49]		
	-1223.8000 ± 2	[37]	96.11000 ± 0.4	[37]
	−1223.8000	(Calc.)	96.11000 ± 0.4	(Calc.)

Table 11
'Lattice stabilities' or Gibbs energy parameters (J/g-atom) of elements [95] $G(\mathrm{Sub}) - G(\mathrm{Ref}) = a_k + b_k T + c_k T\log(T) + d_k T^2 + e_k T^3 + f_k T^{-1}$ for $T_k < T < T_{k+1}$

Name	Ref	T_k	a_k	b_k	c_k	$d_k \times 10^{+3}$	$e_k \times 10^{+6}$	f_k
O_1(L)	O_2(G)	298.15	−2648.9	+31.44				
U_1(ort_A20)	SER	298.15	−8407.734	+130.95515	−26.9182	+1.25156	−4.42605	+38568
		955	−22521.8	+292.121093	−48.66			
U_1(tet)	SER	298.15	−5156.136	+106.976316	−22.841	−10.84475	+0.027889	+81944
		941.5	−14327.309	+244.16802	−42.9278			
U_1(bcc_A2)	SER	298.15	−752.767	+131.5381	−27.5152	−8.35595	+0.967907	+204611
		1049	−4698.365	+202.685635	−38.2836			
U_1(L)	SER	298.15	+3947.766	+120.631251	−26.9182	+1.25156	−4.42605	+38568
		955	−1016663.3	+281.797193	−48.66			

method of transfer of oxygen between oxides which uses a thermobalance.

The homogeneity range of U_4O_9 has been determined by Van Lierde et al. [25] by X-ray analysis, metallography, chemical analysis and electron microscopy. It extends from $O/U = 2.235$ ($x(U) = 0.3091$) to 2.240 ($x(U) = 0.3086$) at 1373 K and from $O/U = 2.235$ ($x(U) = 0.3091$) to 2.245 ($x(U) = 0.3082$) at 298.15 K. U_4O_{9-y} transformed in UO_{2+x} at 1398 K.

The homogeneity range of U_4O_{9-y} (298.15–1073 K) has been measured by Ishii et al. [26] by X-ray diffraction, lattice parameter and the transition temperature methods.

The high- and low-temperature transition in U_4O_9 versus O/U has been studied by Naito et al. [27] by electrical conductivity measurements and X-ray diffraction. The results suggested the existence of three allotropic forms, α-U_4O_{9-y}, β-U_4O_{9-y} and γ-U_4O_{9-y}.

The UO_{2+x} phase boundary with U_4O_{9-y} has been studied by Bannister and Buikx [28] by using a dilatometer which allowed to control and measure the O/U ratio of UO_{2+x} specimen. Phase boundary temperatures were indicated by changes in expansion or contraction rate during heating or cooling, respectively.

The phase boundary UO_{2+x} with U_4O_{9-y} (673–1223 K) has been determined by Saito [29] from electromotive force measurements with cells of the type Ni–NiO/ZrO_2(+CaO)/uranium oxide.

The T–PO_2–(O/U) phase diagram from UO_{2+x} to U_3O_{8-z} (1298–1413 K) has been studied by Matsui and Naito [30] by electrical conductivity measurements and X-ray diffraction. The existence of the hyper-stoichiometric U_4O_{9+y} phase was suggested (1298–1399 K). The homogeneity range of U_4O_{9-y} at room temperature existed from $O/U = 2.228$ ($x(U) = 0.30979$) to $O/U = 2.250$ ($x(U) = 0.30769$).

A two-phase co-existence region $U_8O_{21+x} + U_3O_{8-z}$ in the composition range $2.65 < O/U < 2.67$ has been established by Dharwadkar et al. [31] by micro-thermogravimetric technique, X-ray diffraction and electrical conductivity measurements.

The phase boundaries between U_4O_{9-y} and UO_{2+x}, and U_4O_{9-y} and U_3O_{8-z} have been determined by Picard and Gerdanian [32] from micro-calorimetric measurements of oxygen partial enthalpy, ΔHO_2 at 1323 K.

The nature of the phase diagram for $2.61 < O/U < 2.67$ (800–1400 K) has been established by Caneiro and Abriata [33] from P_{O_2} measurements by thermogravimetric technique. The nearly stoichiometric phase $U_3O_{8\pm z}$ was confirmed, together with a non-stoichiometric U_8O_{21+x} phase stable for $2.617 < O/U < 2.655$. The narrow $U_3O_{8-z} + U_8O_{21+x}$ two-phase region was determined accurately.

The phase boundary UO_{2+x} with U_4O_{9-y} (773–1373 K) has been determined by Nakamura and Fujino [34] by the precise EMF measurements of the solid state galvanic cell of the type NiO/stabilized ZrO_2/UO_{2+x}, at $0.003 < x < 0.23$. Non-stoichiometry x was controlled and determined by the coulometric titration of oxide ions at 1273 K by using NiO in the Ni/NiO reference mixture as a source of oxygen.

The solubility limit of UO_{2+x} (1073–1473 K) has been deduced by Kiukkola [35] from EMF measurements.

The experimental compositions and temperatures of solid–solid equilibria measured by the different authors have been reported in Table 5 ($UO_{2+x} + U_4O_{9-y}$), Table 6 ($UO_{2+x} + U_8O_{21\pm x}$), Table 7 ($U_4O_{9\pm y} + U_8O_{21\pm x}$), Table 8 ($U_8O_{21\pm x} + U_3O_{8-z}$) and Table 9 ($UO_{2+x} + U_3O_{8-z} \Longleftrightarrow U_4O_{9-y}$).

3.2. Thermodynamics

3.2.1. Stoichiometric oxides

The thermodynamic properties of the urania phase have been reviewed by Rand et al. [36], in the framework of a project organized by IAEA, Vienna. The integral thermodynamic data of $UO_{2.00}$ are extensive and consistent. The enthalpy of formation, entropy and heat capacity at room temperature were accepted as $\Delta H_f^0(298.15\,\mathrm{K}) = -1084.9112\ \mathrm{kJ\,mol^{-1}}$, $S_f^0(298.15\,\mathrm{K}) = 77.02744\ \mathrm{J\,mol^{-1}\,K^{-1}}$, $C_p^0(298.15\,\mathrm{K}) = 63.5968\ \mathrm{J\,mol^{-1}\,K^{-1}}$. The heat capacity increases sharply above 1800 K

Table 12
Gibbs energy parameters (J/g-atom) of stable condensed substances (this work) $G(\mathrm{Sub}) - H_{\mathrm{SER}} = a_k + b_k T + c_k T \log(T) + d_k T^2 + e_k T^3 + f_k T^{-1}$ for $T_k < T < T_{k+1}$

Name	T_k	a_k	b_k	c_k	d_k	e_k	f_k
O_2U_1(L)							
	298.15	−1.0183684975e+06	+4.0329181231e+02	−7.4656319589e+01	−6.0984709916e−03	+1.7147239302e−07	+6.4913287914e+05
	1400.00	−1.1390835289e+06	+1.3474087127e+03	−2.0520387032e+02	+5.7013934304e−02	−5.5812076595e−06	+2.1703779530e+07
	2000.00	−1.6100163643e+06	+4.3203803762e+03	−6.0222576124e+02	+2.0458247891e−01	−1.5794767143e−05	+1.2545005974e+08
	2597.97	−1.1160051467e+06	+8.6838091633e+02	−1.3095920000e+02	+0.0000000000e+00	+0.0000000000e+00	+0.0000000000e+00
O_2U_1(S)							
	298.15	−1.1120574111e+06	+4.3388364285e+02	−7.4656319589e+01	−6.0984709916e−03	+1.7147239302e−07	+6.4913287914e+05
	1400.00	−1.2327724425e+06	+1.3780005432e+03	−2.0520387032e+02	+5.7013934304e−02	−5.5812076595e−06	+2.1703779530e+07
	2000.00	−1.7037052778e+06	+4.3509722068e+03	−6.0222576124e+02	+2.0458247891e−01	−1.5794767143e−05	+1.2545005974e+08
	2670.00	−1.3033845812e+06	+1.2187122428e+03	−1.6703783158e+02	+0.0000000000e+00	+0.0000000000e+00	+0.0000000000e+00
	3600.00	+1.0000000000e+06	+0.0000000000e+00	+0.0000000000e+00	+0.0000000000e+00	+0.0000000000e+00	+0.0000000000e+00
O_3U_1(S)							
	298.15	−1.2542745343e+06	+5.0796927469e+02	−8.8700999577e+01	−7.2447998863e−03	+0.0000000000e+00	+5.0451500014e+05
	1500.00	+1.0000000000e+06	+0.0000000000e+00	+0.0000000000e+00	+0.0000000000e+00	+0.0000000000e+00	+0.0000000000e+00
O_8U_3(S)							
	298.15	−3.7570048974e+06	+3.5984680238e+03	−6.1167931056e+02	+5.6012754009e−01	−1.8449640866e−04	+6.1255731166e+06
	430.00	−3.7130672958e+06	+3.8555505193e+03	−6.9162374331e+02	+1.0284934990e+00	−4.1578545194e−04	+0.0000000000e+00
	466.00	−2.1182471119e+08	+4.0934437656e+06	−6.6546706062e+05	+9.4483137476e+02	−2.5166204651e−01	+1.2215996790e+10
	482.28	+2.3768140138e+07	−4.9678793874e+05	+7.9521034880e+04	−1.0316099460e+02	+2.4999846914e−02	−1.7670830200e+09
	520.00	−1.3568444802e+07	+1.7889330560e+05	−2.8588981158e+04	+3.5995755244e+01	−8.5918794943e−03	+6.5113299440e+08
	570.00	+2.9696877315e+07	−5.3352193592e+05	+8.3425234274e+04	−9.3394402393e+01	+1.9544782971e−02	−2.4937438726e+09
	600.00	−2.3728230625e+06	−1.7215055510e+04	+2.6120999667e+03	−2.8695569658e+00	+5.2813235444e−04	−1.0707254838e+08
	700.00	−4.4013299643e+06	+1.1838606414e+04	−1.8400683712e+03	+1.4852064161e+00	−2.7251392903e−04	+6.6730371801e+07
	850.20	−1.2984061608e+06	−2.2608665240e+04	+3.2188770589e+03	−2.3020293964e+00	+2.7938413576e−04	−2.9929206933e+08
	1020.00	−3.6589497868e+06	+1.4647825563e+03	−2.5643531812e+02	−3.0560402537e−02	+1.3265589540e−06	+9.9975196144e+05
	3000.00	+1.0000000000e+06	+0.0000000000e+00	+0.0000000000e+00	+0.0000000000e+00	+0.0000000000e+00	+0.0000000000e+00
O_9U_4(S)							
	298.15	−4.5713348376e+06	+5.5352241533e+02	−1.0422400305e+02	−3.1791388202e−01	+0.0000000000e+00	+0.0000000000e+00
	315.00	−2.1527707153e+07	+4.6262793725e+05	−8.0353134511e+04	+1.6872160812e+02	−6.6861023679e−02	+6.7273171549e+08
	349.10	+6.8263643642e+08	−1.6813679498e+07	+2.8551453398e+06	−5.2734688266e+03	+1.8262229613e+00	−3.1015579491e+10
	358.00	+8.2043672259e+06	−2.9542421960e+05	+4.9607744082e+04	−8.6439240290e+01	+2.8055139701e−02	−6.1593122338e+08
	388.00	−4.5618947011e+06	+7.1984271632e+02	−1.3967700227e+02	−2.6180651252e−01	+5.7985850000e−05	−1.5195273580e+06
	580.00	−4.6208321265e+06	+1.8818657690e+03	−3.2782592349e+02	−5.7467735001e−03	−5.5033983333e−06	+1.7210831177e+06
	1405.00	−4.6153852078e+06	+1.6863234448e+03	−2.9561164282e+02	−4.2621429572e−02	+0.0000000000e+00	+0.0000000000e+00
	1450.00	+1.0000000000e+06	+0.0000000000e+00	+0.0000000000e+00	+0.0000000000e+00	+0.0000000000e+00	+0.0000000000e+00

Table 13
Excess Gibbs energy parameters of condensed solutions $L_{j,k}\langle L\rangle = \sum_v L^v_{j,k}\langle L\rangle (y_j - y_k)^v L_{j,k:l}\langle UO_{2\pm x}, fcc\_C1\rangle = \sum_v L^v_{j,k:l}\langle UO_2 \pm x, fcc\_C1\rangle (y_j - y_k)^v$

Phase	Formula	Parameters
Liquid	$[O_1, O_2U_1, U_1]_1\langle L\rangle$	$L^0[O_1, O_2U_1]_1\langle L\rangle = -75032.40$ $L^1[O_1, O_2U_1]_1\langle L\rangle = -5693.17$ $L^0[O_1, U_1]_1\langle L\rangle = 0$ $L^0[O_2U_1, U_1]_1\langle L\rangle = +28422.83$ $L^1[O_2U_1, U_1]_1\langle L\rangle = -50649.93$ $L^2[O_2U_1, U_1]_1\langle L\rangle = -27846.19$ $L^3[O_2U_1, U_1]_1\langle L\rangle = -25146.41$
$UO_{2\pm x}$, fcc_C1	$[U_1]_1[O_1, Va]_2[O_1, Va]_1\langle UO_{2\pm x}, fcc\_C1\rangle$	$L^0[U_1]_1[O_1, Va]_2[Va]_1\langle UO_{2\pm x}, fcc\_C1\rangle = +164381.63 - 52.87598T$ $L^0[U_1]_1[O_1, Va]_2[O_1]_1\langle UO_{2\pm x}, fcc\_C1\rangle = 0$ $L^0[U_1]_1[O_1]_2[O_1, Va]_1\langle UO_{2\pm x}, fcc\_C1\rangle = -280800.72 - 55.16513T$ $L^1[U_1]_1[O_1]_2[O_1, Va]_1\langle UO_{2\pm x}, fcc\_C1\rangle = -133180.02$ $L^0[U_1]_1[Va]_2[O_1, Va]_1\langle UO_{2\pm x}, fcc\_C1\rangle = 0$ $G(O_3U_1)(fcc\_C1)) - 1.5G(O_2(G)) - G(U_1(ort\_A20)) = -1065703.28 + 272.16504T$ $G(U_1(fcc\_C1)) - G(U_1(ort\_A20)) = +50000$ $G(O_1U_1(fcc\_C1)) - 0.5G(O_2(G)) - G(U_1(ort\_A20)) = +1500000$

and UO_2 undergoes a textural change at 2670 K. The second-order transition is approximated by a first-order one with an enthalpy of transition equal to 1824.224 J at 2670 K. The heat capacity between 2670 K and the melting temperature 3120 K is constant and equal to 167.038 J mol^{-1} K^{-1}; that of UO_2(L) is equal to 130.959 J mol^{-1} K^{-1}. The enthalpy of fusion is $L_f = 74814.104$ J mol^{-1}.

The thermodynamic properties of the other stoichiometric compounds, U_4O_9, U_3O_8 and UO_3 have been reviewed by Cordfunke et al. [37]. The enthalpies of formation at 298.15 K of some uranium oxides have been determined by Mixter [38], Biltz and Fendius [39], Huber et al. [40], Huber and Holley [41], Popov and Ivanov [42] and Fitzgibbon et al. [43] by combining the known enthalpies of formation with data obtained from enthalpy of solution measurements. Other values have been reported by Rand and Kubaschewski [44], Cordfunke and Ailing [45], Vidavskii et al. [46], Duquesnoy and Marion [47], Burdese and Abbattista [48], and Johnson and O'Hare [49].

The heat capacity of U_4O_9 has been experimentally determined by calorimetry by Osborne et al. [50] from 5 to 310 K, by Gotoo and Naito [51] from 300 to 520 K, by quasi-adiabatic technique by Westrum and Takahashi [52] from 190 to 400 K, by adiabatic calorimetry by Gronvold et al. [53] from 300 to 1000 K, by adiabatic vacuum drop calorimetry by MacLeod [54] from 800 to 1600 K, by adiabatic calorimetry by Inaba and Naito [55] from 180 to 470 K. A λ-type anomaly was observed with a maximum at 330 K, and an associated enthalpy of transition equal to 2845 J mol^{-1} [51], 348 K, 2510 ± 33 J mol^{-1} [52], 348 K, 2760 ± 280 J mol^{-1} [53], 2427 J mol^{-1} [54], 342 K, 2527 ± 50 J mol^{-1} [55], 348 K, 2594 J mol^{-1} [37]. A small irregularity in the heat capacity was observed in the region 900–950 K with an entropy increment of 0.15 J mol^{-1} K^{-1}. An order–disorder transition occurs at 1398 ± 8 K with an associated enthalpy increment of 9372 ± 418 J mol^{-1} [54], 1400 K and 11900 J mol^{-1} [37].

The heat capacity of U_3O_8 has been experimentally determined by calorimetry by Popov et al. [56] from 380 to 707 K, Girdhar and Westrum [57] from 300 to 555 K, Maglic and Herak [58] from 273 to 1000 K, by adiabatic scanning calorimetry by Inaba et al. [59] from 310 to 970 K.

A reversible λ-type anomaly was observed at 482.7 K with an enthalpy of transition of 172 ± 4 J mol^{-1} [56], 481 K [57]. Three λ-type anomalies were observed at 483, 568 and 850 K, indicating second-order phase transitions, with associated enthalpies of transition of 405 ± 21, 444 ± 21, 942 ± 81 J mol^{-1} [58] assessed by Cordfunke et al. [37].

The heat capacity of UO_3 has been experimentally determined by drop calorimetry by Moore and Kelley [60] from 415 to 900 K, Popov et al. [56] from 382 to 673 K, Jones et al. [61] from 15 to 295 K, Cordfunke and Westrum [62] by adiabatic calorimetry from 350 to 700 K.

The enthalpy of formation and entropy at room temperature from different authors have been reported in Table 10.

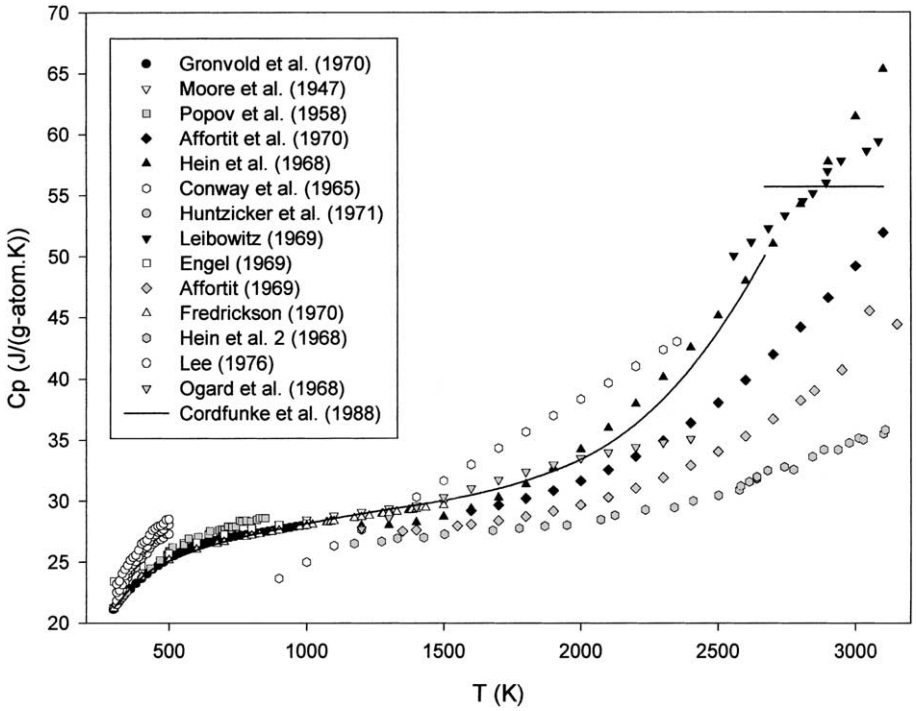

Fig. 1. Calculated heat capacity of $O_2U_1(S)$ compared to selected experimental values.

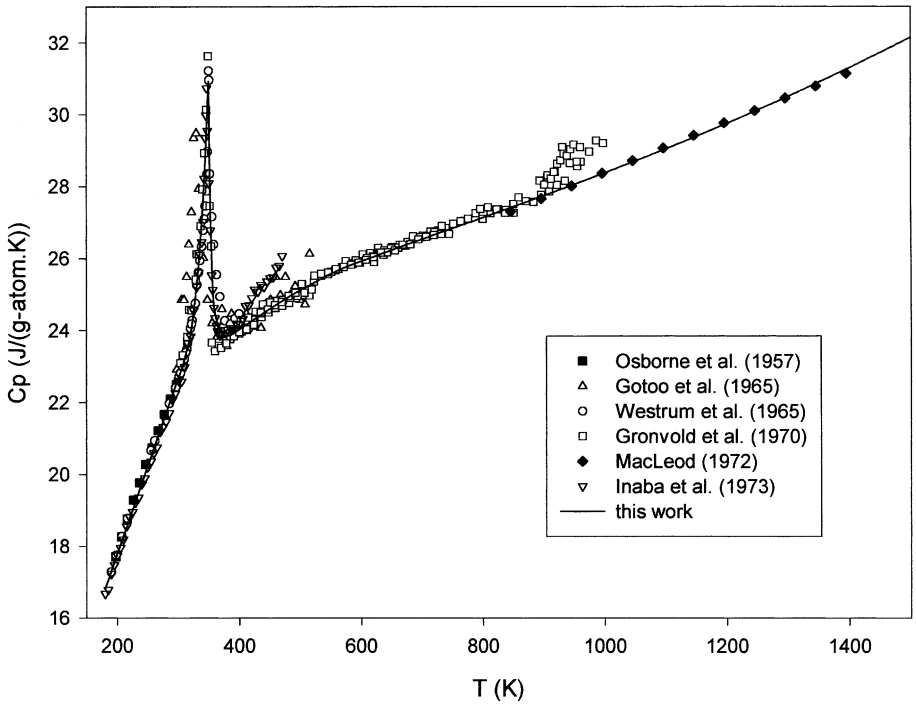

Fig. 2. Calculated heat capacity of $O_9U_4(S)$ compared to selected experimental values.

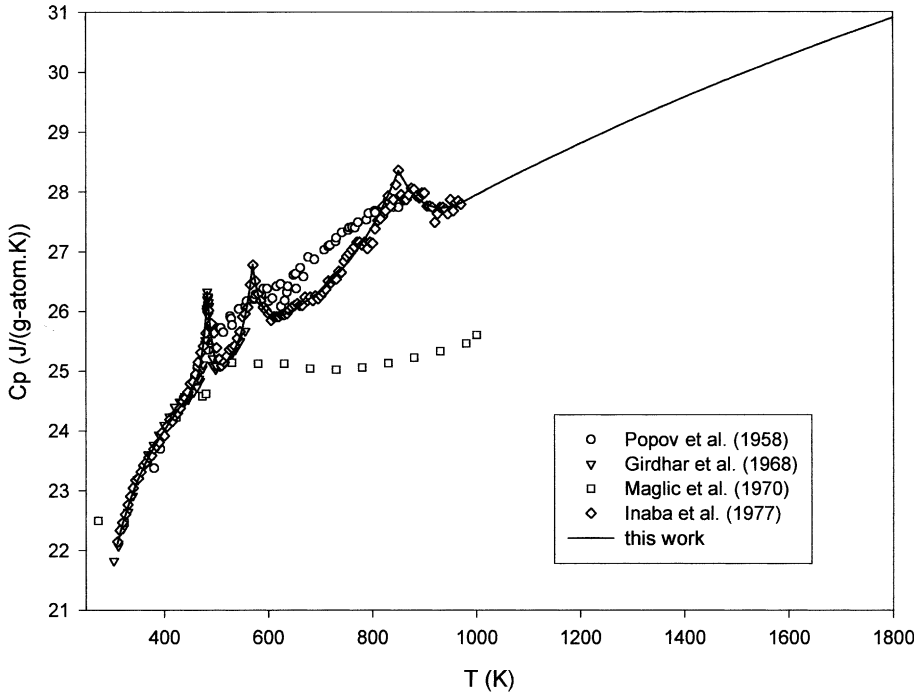

Fig. 3. Calculated heat capacity of $O_8U_3(S)$ compared to selected experimental values.

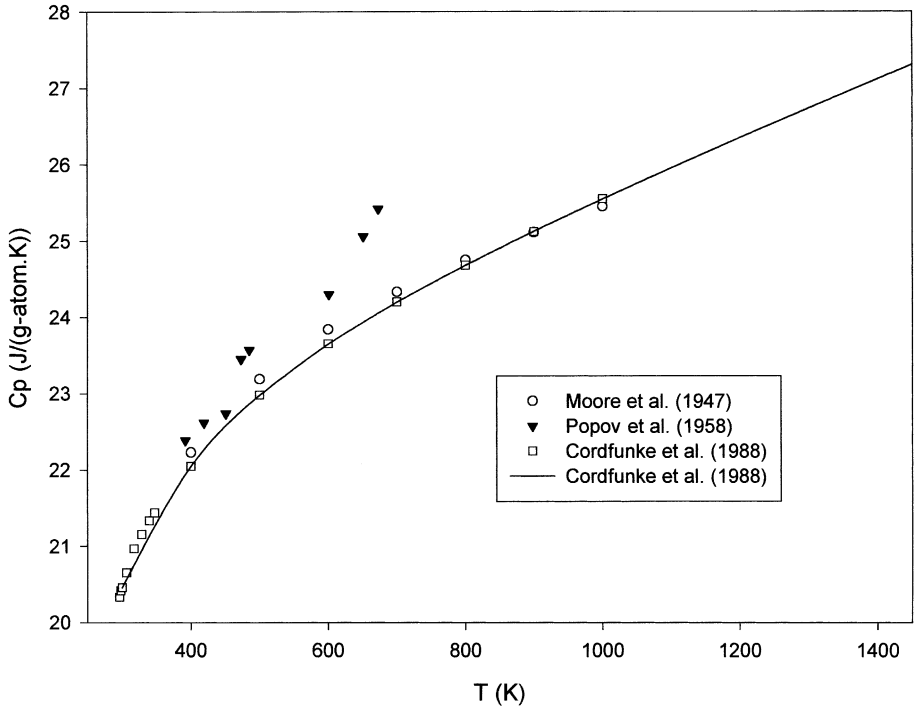

Fig. 4. Calculated heat capacity of $O_3U_1(S)$ compared to selected experimental values.

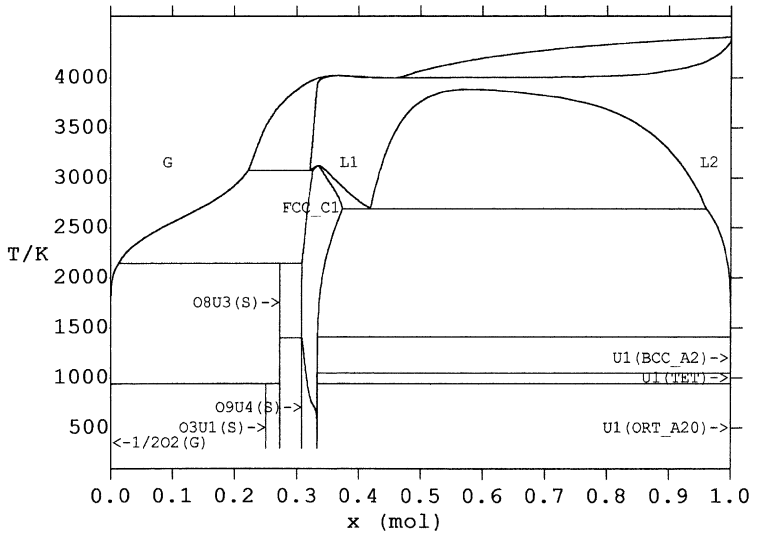

THREE-PHASE REACTIONS

1407.90	1.000	1.000	0.334
2692.00	0.419	0.960	0.374
1049.00	1.000	1.000	0.333
942.02	1.000	1.000	0.333
2148.20	0.273	0.309	0.126
940.88	0.000	0.250	0.273
1400.00	0.308	0.308	0.273
3076.90	0.326	0.321	0.222

TRANSITIONS

3120.00	0.333
942.00	1.000
1049.00	1.000
1408.00	1.000
4408.00	1.000

Fig. 5. Calculated O–U phase diagram ($P = 1$ atm) with invariant reactions or special points.

3.2.2. Chemical potential of oxygen

In the following, ΔGO_2 ($J\,mol^{-1}$) is the chemical potential of diatomic oxygen (oxygen potential) referred to $O_2(G)$: $\Delta GO_2 = RT \ln P_{O_2}$, where P_{O_2} is the partial pressure of $O_2(G)$, expressed in atmosphere. In the O–U binary system, the chemical potential of monoatomic oxygen referred to 0.5 $O_2(G)$ is defined by ΔGO (J/mol) $= 0.5\,\Delta GO_2$ (J/mol) $= RT \ln a(O)$; $a(O)$ is the activity of oxygen in the O–U binary system, referred to 0.5 $O_2(G)$.

The entire $UO_{2\pm x}$ database for the dependence of the non-stoichiometry, x, on temperature and oxygen potential, was retrieved from the literature for the first time by Lindemer and Besmann [63]. This database was interpreted by least-squares analysis using equations derived from the classical thermodynamic theory for the solid solution of a solute in a solvent. This analysis was the first mathematical representation of thermodynamic properties of $UO_{2\pm x}$, but did not consider the other phases and the self-consistency with phase diagram informations. This compilation has been directly used in the present work.

3.2.2.1. Hypo-stoichiometric field. A new technique of gas equilibration in a sealed silica system has been developed by Markin et al. [64] to obtain UO_{2-x} data for $2200 < T < 2400$ K.

Measurements of oxygen partial pressures over UO_{2-x}, including the region close to stoichiometry, have been made by Tetenbaum and Hunt [11,12] for $2080 < T < 2705$ K. The oxygen potential of the carrier gases were fixed by using the transpiration method with flowing H_2–H_2O mixtures.

Oxygen chemical potentials for UO_{2-x} have been measured at 1800, 1900 and 2000 K by Wheeler [65], by using a technique in which the UO_{2-x} sample was equilibrated in an oxygen potential controlled by the equilibrium: $2C + O_2 \Longleftrightarrow 2CO$.

Transpiration experiments have been performed by Javed [66] to study the thermodynamics of hypo-stoichiometric urania. The oxygen partial pressures were fixed with flowing H_2/H_2O mixtures. After equilibration, the quenched products were analysed by chemical, X-ray and metallographic techniques. The oxygen chemical potential of UO_{2-x} versus x was given at 1873, 1973, 2073 and 2173 K.

Measurements of vapor pressures of gaseous species have been performed by Pattoret et al. [84] for $1.9 < O/U < 2$ and $1700 < T < 2500$ K by effusion and mass spectrometry.

The limiting composition under free vaporisation as a function of temperature and oxygen partial pressure has been determined by Aitken et al. [86]. They also used a tantalum container as an inert membrane which allowed a UO_2 specimen to reach equilibrium with the outside atmosphere by the passage of oxygen through the tantalum ($1.8702 < O/U < 1.9942$ and $2023 < T < 2873$ K).

3.2.2.2. Hyper-stoichiometric field. Data for UO_{2+x} for $1600 < T < 1700$ K have been obtained by Markin et al. [64] with the technique of gas equilibration in a sealed silica system.

The oxygen chemical potential of UO_{2+x} in the field $2.01 < O/U < 2.2$, $1150 < T < 1350$ K has been determined by Aronson and Belle [67] from EMF measurements on uranium oxide half-cells. The cells were of the

Table 14
Gibbs energy parameters (J/mol) of gaseous species, limited to 6000 K (COACH [98]) $G(\mathrm{Sub}) - G(\mathrm{Ref}) = a_k + b_k T + c_k T\log(T) + d_k T^2 + e_k T^3 + f_k T^{-1}$ for $T_k < T < T_{k+1}$

Name	T_k	a_k	b_k	c_k	d_k	e_k	f_k
O_1(G)							
	298.15	+2.4315271223e+05	−1.9768353956e+01	−2.1187789894e+01	+3.1192657423e−04	−4.4743109082e−08	−3.9429214725e+04
	1200.00	+2.4277575832e+05	−1.8029781131e+01	−2.1393571775e+01	+2.6307403526e−04	−2.1018747482e−08	+4.5566418264e+04
	4200.00	+2.5615326700e+05	−6.2660801072e+01	−1.5958230064e+01	−7.2232471677e−04	+1.2502099791e−08	−6.1799306436e+06
O_2(G)							
	298.15	−7.0602882651e+03	−4.9152832099e+01	−2.2588296136e+01	−9.7947960689e−03	+1.2353059908e−06	−7.1500115612e+04
	1100.00	−1.3083001915e+04	+2.5071616144e+01	−3.3615486270e+01	−1.1813636232e−03	+1.1634396981e−08	+5.1020407218e+05
	3500.00	+1.3373055271e+04	−4.9966787673e+01	−2.4652391914e+01	−2.6191717530e−03	+5.9896337111e−08	−1.4469647464e+07
O_3(G)							
	298.15	+1.3184401713e+05	−6.1993243331e+01	−2.3638029683e+01	−3.3297965924e−02	+6.0468791438e−06	+4.0072252494e+04
	700.00	+1.1528963785e+05	+1.7102911110e+02	−5.9292523898e+01	+1.5400082084e−03	−4.5818986202e−07	+1.5115994127e+06
	1400.00	+5.7220635930e+04	+6.5707208335e+02	−1.2720323834e+02	+3.6802948955e−02	−3.8868110847e−06	+1.0816764021e+07
	2300.00	+1.1480034113e+06	−4.8545219108e+03	+5.8512182213e+02	−1.7071315510e−01	+7.4899464204e−06	−3.0353954198e+08
	3400.00	−1.9113615418e+06	+6.2397594274e+03	−7.8152668489e+02	+1.0125660312e−01	−2.6809850377e−06	+9.8372401000e+08
	4900.00	−2.3068802126e+05	+1.6865401835e+03	−2.4271445722e+02	+2.4437807370e−02	−6.2659916640e−07	+0.0000000000e+00
O_1U_1(G)							
	298.15	+8.5092021960e+03	−5.6900151336e+01	−2.8376252134e+01	−7.9532902671e−03	+1.3374135150e−06	+5.8782585000e+04
	900.00	+3.8847353654e+03	+2.4914484585e+00	−3.7328246151e+01	−1.6817123555e−05	+5.6409176273e−10	+5.2997263600e+05
O_2U_1(G)							
	298.15	−5.0266728973e+05	−3.6612685831e+01	−3.5043698847e+01	−2.3055283480e−02	+4.4783715890e−06	+1.3102702243e+05
	700.00	−5.1272296825e+05	+1.0894889217e+02	−5.7448621618e+01	−2.1946711760e−04	+1.1384531507e−08	+1.0051273366e+06
	3700.00	−5.1183333989e+05	+1.1049037488e+02	−5.7719953600e+01	−3.6591590400e−05	+0.0000000000e+00	+0.0000000000e+00
O_3U_1(G)							
	298.15	−8.2207493375e+05	+1.3469596388e+02	−6.4408545252e+01	−1.5889700244e−02	+2.5374768887e−06	+3.5681975451e+05
	1000.00	−8.3171879176e+05	+2.6312564731e+02	−8.3759091680e+01	+7.3969884218e−04	−6.6393412901e−08	+1.2143047874e+06
	1600.00	−8.3083319874e+05	+2.5590945704e+02	−8.2745170917e+01	+1.7353684872e−04	−5.6887410089e−09	+1.0419833231e+06
U_1(G)							
	298.15	+5.1859170123e+05	+1.3908624797e+01	−3.2542315284e+01	+1.1279854842e−02	−2.4286028070e−06	+1.5190430400e+05
	1000.00	+5.4014082978e+05	−2.0181340371e+02	−1.4447352000e+00	−9.0591968628e−03	+1.1778657403e−07	−2.6970064000e+06
	2200.00	+5.7537873757e+05	−4.1603165833e+02	+2.6972156000e+01	−1.9057492358e−02	+7.6790346667e−07	−1.0691375200e+07
	3800.00	+2.3772000934e+05	+6.9331218572e+02	−1.0784929398e+02	+5.0126412000e−03	−4.2475270527e−08	+1.4886253600e+08
	4100.00	+1.9452121614e+05	+8.0155056149e+02	−1.2051405094e+02	+6.6447359409e−03	−8.1749084000e−08	+1.7611773960e+08

type Fe, $FeO/ZrO_2 + CaO/UO_{2+x}$, Pt where x varied from 0.01 to 0.20.

The volatility of UO_{2+x} and the phase relations has been studied by Chapman and Meadows [68] by using thermogravimetric techniques. Chemical reactions describing the loss of uranium from UO_{2+x} ($1373 < T < 2473$ K, $10^{-6} < PO_2 < 10^2$ Torr) were proposed, and results obtained required the consideration of $UO_4(G)$ as the uranium-bearing vapor species above UO_{2+x}. The equilibrium oxygen pressures were measured in the field $2.01 < O/U < 2.63$, $1271 < T < 1774$ K.

The non-stoichiometry in the phases UO_{2+x} and U_8O_{21-x} has been determined as a function of the partial oxygen pressure by Hagemark and Broli [23] by use of a thermobalance. The oxygen chemical potential was tabulated in the field $2.010 < O/U < 2.225$ and $2.615 < O/U < 2.625$, $1173 < T < 1773$ K.

Electromotive force measurements on high-temperature solid electrolyte galvanic cells containing solid electrolyte have been successively carried out by Marchidan and Matei [69], Marchidan and Matei-Tanasescu [70] and Marchidan and Tanasescu [71,72], in order to obtain thermodynamic data in the hyper-stoichiometric domain. The oxygen chemical potential was tabulated versus x in the UO_{2+x}, $UO_{2+x} + U_4O_{9-y}$ and $U_4O_{9-y} + U_8O_{21\pm x}$ fields for $1073 < T < 1373$ K.

Thermodynamic properties of uranium oxides, principally in the non-stoichiometric UO_{2+x} single-phase region, have been determined by electromotive force measurements with cells of the type $Ni–NiO/ZrO_2(+CaO)$/uranium oxide by Saito [29] in the field $2.04 < O/U < 2.34$, 773–1373 K. The relative partial molar free energies of oxygen for the single-phase region UO_{2+x} and the two-phase coexisting regions $UO_{2+x} - U_4O_{9-y}$ and $U_4O_9 - U_8O_{21\pm x}$ were obtained with adequate precision. The chemical oxygen potential of UO_{2+x} was tabulated versus x for $973 < T < 1473$ K.

The oxygen chemical potential of UO_{2+x} versus x has been determined theoretically by Naito and Kamegashira [73] for $1073 < T < 1773$ K.

The partial molar mixing enthalpy of oxygen, ΔHO_2, in uranium oxides has been determined by Picard and Gerdanian [32] by using the microcalorimetric method in the field $2 < O/U < 2.6$, $T = 1323$ K. The oxygen potential chemical potential of UO_{2+x} was given at 1355 and 1323 K.

A complete set of thermodynamic parameters of UO_{2+x} – the relative partial molar thermodynamic quantities of oxygen gO_2, hO_2, sO_2 as a function of non-stoichiometry x and temperature T – has been determined by Nakamura and Fujino [34]. The chemical oxygen potential of UO_{2+x} versus x at $T = 1273$ K was tabulated.

The oxygen partial pressure over both hypo- and hyper-stoichiometric compositions has been deduced by Chapman et al. [74] from induction heating measurements in controlled H_2O/H_2 and CO_2/CO gas mixtures and direct internal zone melting, at 2200 K (fcc_C1) and 3150 K (liquid).

The oxygen chemical potential of UO_{2+x} versus x has been determined by Kiukkola [35] by the EMF method for $1073 < T < 1473$ K.

Hyper-stoichiometric urania ($O/U = 2.035$, 2.045) have been submitted by Adamson and Carney [75] to thermal gradients in a CO/CO_2 atmosphere and oxygen potential have been measured between 1623 and 1773 K.

The oxygen potential of UO_{2+x} has been measured by Une and Oguma [76] by a the EMF method for $973 < T < 1373$ K, $x = 0$–0.11, and by Une and Oguma [77] by thermogravimetric technique in CO/CO_2 atmosphere at 1273, 1573 and 1773 K, $x = 0$–0.08.

The oxygen potential has been determined by the EMF method by Schleifer et al. [78] at 1250 K ($x = 0.005$–0.025).

Thomas et al. [79] have determined the oxygen potential of UO_{2+x} ($2.0014 < O/U < 2.04$) by using CO/CO_2 mixtures and a thermobalance from 1173 to 1423 K.

The equilibrium oxygen pressure at 1950 K and $1.995 < O/U < 2.005$ has been determined by Wheeler and Jones [80] under different atmospheres (CO, CO/CO_2, H_2/H_2O) and with different crucibles (graphite, molybdenum).

The oxygen partial pressures over UO_{2+x} ($2 < O/U < 2.15$, $1176 < T < 1373$ K) have been measured by Gerdanian and Dodé [81] by using a thermobalance in a controlled CO/CO_2 atmosphere.

The low values of P_{O_2} ($2.0039 < O/U < 1.9991$, $973 < T < 1273$ K) have been obtained by Baranov and Godin [82] by using a closed solid electrolyte, with the aid of a ceramic pump.

The oxygen pressure over UO_{2+x} and $UO_{2+x} + U_4O_{9-y}$ has been measured by Markin et al. [83] by the EMF method using galvanic cells for $2.01 < O/U < 2.6$ and $723 < T < 1333$ K.

P_{O_2} values ($0.315 < x(U) < 0.3333$, $1373 < T < 1673$ K) have been determined by Aukrust et al. [85] by using gas mixtures CO_2/CO or O_2/Ar for obtaining proper oxygen pressures and a thermogravimetric method for the non-stoichiometry.

4. Thermodynamic modelling

4.1. Substances

In the classical substance databases, the fundamental thermodynamic properties stored for a substance are the enthalpy of formation $\Delta H^0_{f,298.15\,K}$ and the entropy at room temperature $S^0_{298.15\,K}$, the heat capacity C^0_p at constant pressure varying versus temperature T, expressed in Kelvin, according to the relation (1), and the transi-

tion enthalpy L_{tr} if the substance shows a structural transformation at the temperature T_{tr}.

$$C_p^0 = C_k + D_kT + E_kT^2 + F_kT^{-2} + \cdots + G_kT^3 + H_kT^4 + I_kT^6 + J_kT^{-10} + L_kT^{-3} + M_kT^{-4} \quad \text{for } T_k < T < T_{k+1}. \tag{1}$$

In the format used for phase diagrams calculations, the stored quantity is the Gibbs energy of the substance Φ, $G - H_{SER}$, referred to a given reference state. SER means 'stable element reference' and is defined by the use of $H_{298.15\,K}$ and $S_{0\ K}$ for the stable state of the pure elements at 298.15 K and 1 bar. It is possible to calculate directly this quantity from the fundamental thermodynamic values, and reciprocally.

$$G - H_{SER} = a_k + b_kT + c_kT\log T + d_kT^2 + e_kT^3 + f_kT^{-1} + \cdots + g_kT^4 + h_kT^5 + i_kT^7 + j_kT^{-9} + k_k\log T + l_kT^{-2} + m_kT^{-3}) \quad \text{for } T_k < T < T_{k+1}. \tag{2}$$

In this expression, the coefficients $c, d, e, f, \ldots$ are connected to those of the heat capacity, while a and b are two integration constants depending on all the fundamental thermodynamic values. The points of suspension mean that these extra terms may be added if necessary, and are often used for extrapolation outside the stable domain.

In this work, these two analytical expressions (1) and (2), have been used for describing the heat capacity and the Gibbs energy of the stoichiometric compounds O_3U_1(S), O_8U_3(S) and O_9U_4(S).

4.2. Solutions

In a general way, the Gibbs energy of a condensed solution phase is the sum of several terms: reference, ideal, excess and magnetism or ordering in some cases.

$$G = G^{Ref} + G^{Id} + G^{Ex}(+G^{Mag} + G^{Ord}). \tag{3}$$

In this work, the general multisublattice model, presented by Sundman and Agren [87], has been used for the condensed solution phases, i.e. the liquid phase, L, and the non-stoichiometric solid solution, $UO_{2\pm x}$. The very narrow non-stoichiometry ranges of U_4O_{9-y} and U_3O_{8-z} have been neglected in a first approximation.

4.2.1. Liquid

The liquid phase is represented by means of the associate model, basically described by Dolezalek [88], followed by Prigogine and Defay [89], and included in the previous formalism. It is supposed to be a non-ideal mixture of pure species O_1(L) and U_1(L), and associated species O_2U_1(L), and thus represented by the formula: $[O_1, U_1, O_2U_1]_1\langle L\rangle$.

$$G^{Ref}(L) = yO_1^0G(O_1^L) + yU_1^0G(U_1^L) + yO_2U_1^0G(O_2U_1^L), \tag{4}$$

$$G^{Id}(L) = RT(yO_1Lnyo_1 + yU_1Lnyu_1 + yO_2U_1Lnyo_2u_1), \tag{5}$$

in which R is the perfect gas constant.

$$G^{Ex}(L) = yO_1yU_1L[O_1, U_1]_1\langle L\rangle + yO_1yO_2U_1L[O_1, O_2U_1]_1\langle L\rangle + yU_1yO_2U_1L[U_1, O_2U_1]_1\langle L\rangle, \tag{6}$$

with $y(i) = n(i)/\sum n(i)$.

The binary interaction parameters between j and k species, $L_{j,k}\langle L\rangle$ are described by using a Redlich–Kister type polynomial expression [90].

$$L_{j,k}\langle L\rangle = \sum\nolimits_v L_{j,k}^{(v)}\langle L\rangle(y_j - y_k)^v. \tag{7}$$

The $L_{j,k}^{(v)}\langle L\rangle$ parameters may vary with temperature similarly to relation (2).

4.2.2. $UO_{2\pm x}$, fcc_C1

The $UO_{2\pm x}$ solid solution is represented by a sublattice model, with defects which allow to describe both hypo- and hyper-stoichiometric fields.

The stoichiometric compound UO_2 has the face-centered cubic structure C1, noted fcc_C1, of CaF_2 (fluorite) type, Fm3m, cF_{12}: its formula may be written as $[U]_1[O_1]_2\langle UO_2$, fcc_C1$\rangle$.

The structure analysis of $UO_{2\pm x}$ has been made by Willis [91,92].

For UO_{2-x}, the presence of vacancies (Va) on the oxygen sublattice allows one to describe the hypo-stoichiometric field: its formula may be written $[U]_1[O_1, Va]_2\langle UO_{2-x}$, fcc_C1$\rangle$, the solid solution being possible between the two reference substances, stable O_2U_1(fcc_C1) and fictive U_1(fcc_C1).

For UO_{2+x}, two defects models are possible to describe the hyper-stoichiometric field: vacancies on the uranium sublattice, Va, or interstitial of excess oxygen in the fcc_C1 structure. The first one was previously chosen by [1], who used the formula $[U_1, Va]_1[O_1, Va]_2\langle UO_{2\pm x}$, fcc_C1$\rangle$ for the whole domain. However, numerous data show that the predominant defects are oxygen vacancies and interstitial oxygen ions, both of which probably form clusters, even at low defect concentrations [37,73]. Thus, there exist three kinds of oxygen, O, O_i^a, and O_i^b: the first one is the regular site for fluorite type UO_2 and is partially vacant, the two others are interstitial. Thus, UO_{2+x} contains three kinds of defects, which agglomerate into complex clusters $Va–O_i^a–O_i^b$. A possible general formula could be $[U]_1[O,Va]_2[O_i^a, Va]_2[O_i^b, Va]_2\langle UO_{2\pm x}$, fcc_C1$\rangle$ or $[U]_1[O,Va]_2[O_i^a, Va]_1[O_i^b, Va]_2\langle UO_{2\pm x}$, fcc_C1$\rangle$. According Matsui and Naito [93], different defects

models considering interactions were proposed, depending on the oxygen pressure (low, intermediate, high) and temperature levels.

Our aim being to establish the best consistency between phase diagram and thermodynamic properties (oxygen potential in particular), we will use a simplified three sublattice model for $UO_{2\pm x}$, with the formula $[U_1^{(1)}]_1[O_1^{(2)}, Va^{(2)}]_2[O_1^{(3)}, Va^{(3)}]_1\langle UO_{2\pm x}, fcc\_C1\rangle$, which does not distinguish the two types of interstitial oxygen, neither give more precise structural informations. The possibility of estimating interaction terms between O and Va allows one to describe accurately the dependence of P_{O_2} with x and T in both hypo- and hyper-stoichiometric fields.

$$\begin{aligned} G^{Ref}(UO_{2\pm x}, fcc\_C1) = {} & yO_1^{(2)}yO_1^{(3)0}G(O_3U_1^{fcc\_C1}) \\ & + yO_1^{(2)}yVa^{(3)0}G(O_2U_1^{fcc\_C1}) \\ & + yVa^{(2)}yO_1^{(3)0}G(O_1U_1^{fcc\_C1}) \\ & + yVa^{(2)}yVa^{(3)0}G(U_1^{fcc\_C1}). \end{aligned} \quad (8)$$

In this expression, $O_2U_1^{fcc\_C1}$ is the stable reference compound, while $O_3U_1^{fcc\_C1}$, $O_1U_1^{fcc\_C1}$ and $U_1^{fcc\_C1}$ are fictive metastable reference compounds.

$$\begin{aligned} G^{Id}(UO_{2\pm x}, fcc\_C1) = {} & 2RT(yO_1^{(2)}LnyO_1^{(2)} + yVa^{(2)}LnyVa^{(2)}) \\ & + RT(yO_1^{(3)}LnyO_1^{(3)} + yVa^{(3)}LnyVa^{(3)}), \end{aligned} \quad (9)$$

$$\begin{aligned} & G^{Ex}(UO_{2\pm x}, fcc\_C1) \\ & = yO_1^{(3)}yO_1^{(2)}yVa^{(2)}L[U_1^{(1)}]_1[O_1^{(2)}, Va^{(2)}]_2[O_1^{(3)}]_1\langle ss\rangle \\ & + yVa^{(3)}yO_1^{(2)}yVa^{(2)}L[U_1^{(1)}]_1[O_1^{(2)}, Va^{(2)}]_2[Va^{(3)}]_1\langle ss\rangle \\ & + yO1^{(2)}yO_1^{(3)}yVa^{(3)}L[U_1^{(1)}]_1[O_1^{(2)}]_2[O_1^{(3)}, Va^{(3)}]_1\langle ss\rangle \\ & + yVa^{(2)}yO_1^{(3)}yVa^{(3)}L[U_1^{(1)}]_1[Va^{(2)}]_2[O_1^{(3)}, Va^{(3)}]_1\langle ss\rangle \end{aligned} \quad (10)$$

with

$$L_{j,k:l}\langle UO_{2\pm x}, fcc\_C1\rangle = \sum\nolimits_v L_{j,k:l}^{(v)}\langle ss\rangle(y_j - y_k)^v. \quad (11)$$

ss is used for $UO_{2\pm x}$, fcc_C1. $L_{j,k:l}$ represents the interaction parameter between the components j and k of one sublattice, the second sublattice (if existing) being supposed completely fulfilled by the component l. The $L_{j,k:l}^{(v)}\langle UO_{2\pm x}, fcc\_C1\rangle$ parameters may vary with temperature similarly to relation (2).

5. Critical assessment method and Gibbs energy parameters

The values used for the lattice stabilities of the pure condensed elements have been taken from the SGTE database [94,95] for the following stable or metastable structures: O_1(L), U_1(L), U_1(bcc_A2), U_1(tet), U_1(ort_A20), and are reported in Table 11.

The thermodynamic data of pure oxide UO_2(fcc_C1, L) were already assessed [1] and fixed in the following. The c_k, d_k, e_k, f_k heat capacity coefficients of the three other binary stoichiometric substances O_9U_4(S), O_8U_3(S) and O_3U_1(S) were assessed separately in the following subsection. The enthalpy and entropy coefficients a_k and b_k were critically assessed from the compiled thermodynamic and phase diagram data. The Gibbs energy parameters of these four compounds are reported in Table 12.

The critical assessment of the coefficients, a_k and b_k for the three previous stoichiometric substances, or other metastable reference substances, U_1(fcc_C1), O_1U_1(fcc_C1), and O_3U_1(fcc_C1), and of the binary interaction parameters $L_{j,k}^{(v)}$ and $L_{j,k:l}^{(v)}$ for the liquid and $UO_{2\pm x}$, fcc_C1 solid solution, was performed by using the optimisation program developed by Lukas et al. [96], which allows one to take into account simultaneously all the available experimental information, equilibrium phase diagram and thermodynamic properties, after a primary criticism. The solution interaction parameters and associated reference substances are reported in Table 13. Details of the optimisation process are given in the next subsections.

5.1. Thermodynamic data for stoichiometric oxides

The thermodynamic properties of stoichiometric urania UO_2(S, L) reviewed by Rand et al. [36] have been retained, i.e. $\Delta H^0_{f(298.15\,K)}$, $S^0_{f(298.15\,K)}$, $C^0_{p(298.15\,K)}$, $C_p(T)$, T^{tr}(S), L^{tr}(S), T^f, L^f. The heat capacity of the solid above the melting point was kept constant. The heat capacity of the liquid below the melting point was kept constant down to the glass transition estimated at 2598 K. The selected heat capacity of UO_2 is presented on Fig. 1.

The heat capacity of the three other stoichiometric compounds, O_9U_4(S), O_8U_3(S) and O_3U_1(S) was assessed from all existing experimental values after a primary criticism and presented on Figs. 2–4 respectively.

Contrary to Cordfunke et al. [37], the λ-type anomaly of O_9U_4(S) and the three λ-type anomalies of O_8U_3(S) are correctly represented as second-order transition without associated first-order enthalpy. The other anomalies for O_9U_4(S) in the temperature ranges 400–550 and 900–950 K were not taken into account.

The enthalpy and entropy of formation of these three compounds have been optimised from all the compiled experimental values and also from solid–solid equilibria which impose some constraints, especially invariant reactions such as the peritectoid one $UO_{2+x} + U_3O_{8-z} \Longleftrightarrow U_4O_{9-y}$. The assessed values are given in Table 10.

5.2. Primary selection of experimental data

5.2.1. Phase diagram data

The liquidus and solidus above the monotectic temperature in the oxide domain have been determined by Bates [8] (±30 K), Bannister [9] (±70 K), and Latta and Fryxell [13] (±15 K). Thus, the last data, which included also the hyper-stoichiometric field, were preferred. However, the other data were also used with a lower weight in the optimisation procedure, and surimposed on the calculated phase diagram.

The solidus below the monotectic temperature has been determined by Bates [4], Martin and Edwards [5], Blum et al. [6], Ackermann et al. [10], Tetenbaum and Hunt [11,12], Ackermann and Rauh [15]. Only the data of Bates [4] were found to be less consistent with all others, and their weights were lowered in the optimisation procedure.

The liquidus below the monotectic reaction was determined by Martin and Edwards [5], Blum et al. [6], Guinet et al. [7] and Garg and Ackermann [14], but showed a great discrepancy.

Guinet et al. [7] redetermined their previous results [6] and explained in detail the encountered experimental difficulties: "*they are mainly due to the existence of a thermal gradient between the crucible and the bath... Only a cooling which maintains the homogeneity of temperature in the liquid allows to precipitate the molten dioxide in its mass*".

According to Garg and Ackermann [14], "*the difference is mainly due to the different methods employed for quenching and sampling*", and that is why they used a simple method, developed by Ackermann and Rauh [15] and Garg and Ackermann [16], which did not involve post-experimental evaluation of the quenched sample.

Taking into account the analysis of the experimental methods, the liquidus of Blum et al. [6] and Guinet et al. [7] have been 'a priori' discarded. However, a discrepancy still remains between the results of Martin and

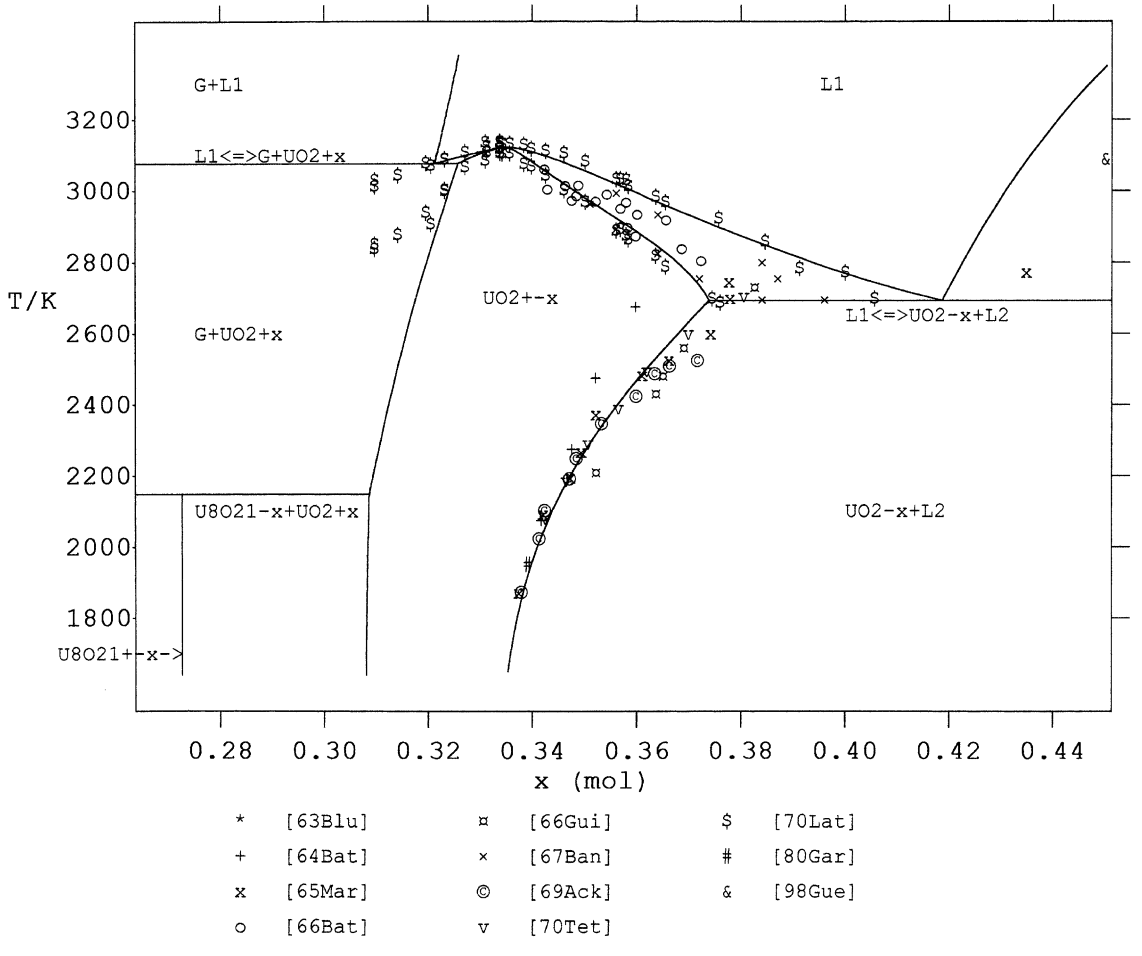

Fig. 6. Partial O–U phase diagram ($UO_{2\pm x}$ region) compared to various experimental points.

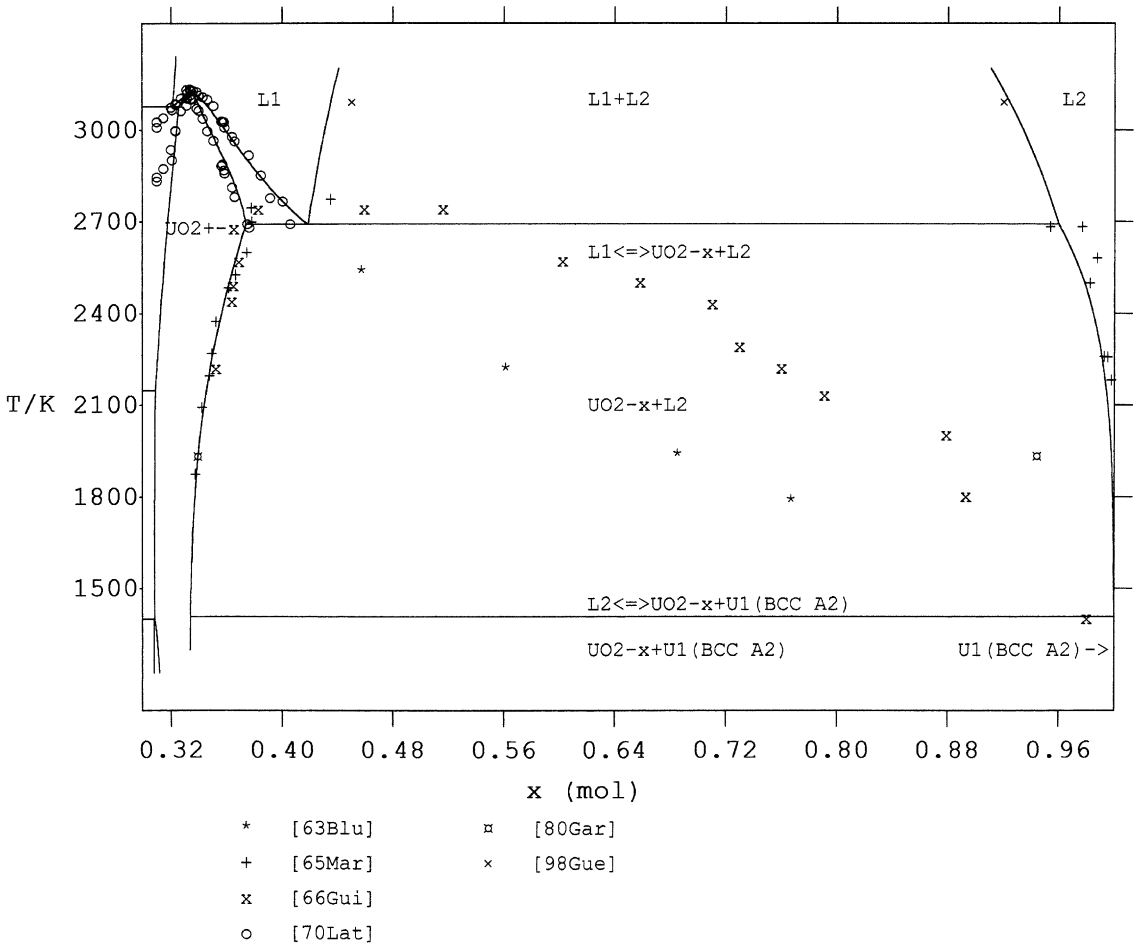

Fig. 7. Partial O–U phase diagram ($UO_{2\pm x}$ – U region) compared to various experimental points.

Edwards [5] and Garg and Ackermann [14]. On the basis of the new experimental results on the liquid miscibility gap in the O–U binary system and the O–U–Zr ternary system reported by Gueneau et al. [17], the measured composition of L_2 at high temperature ($x^{L_2}(U) = 0.98$ at 3090 ± 100 K) argued for the assumption of a low solubility of oxygen at lower temperature. Moreover, measurements of the solubility of oxygen in U–Zr alloys in the temperature range 1973–2173 K by Maurisi et al. [97] indicate also a low solubility of oxygen. Consequently, the Garg and Ackermann [14] results were also discarded, while the older results of Martin and Edwards [5] were selected. Nevertheless, we still think that it would be necessary to have concluding experiments around 2000 K for such an important feature of the diagram.

The solid–solid equilibria in the hyper-stoichiometric field show a good consistency. The diphasic UO_{2+x}–U_4O_{9-y} and $UO_{2+x} - U_8O_{21\pm x}$ domains have been extensively studied up to 1900 K. The only uncertainty is the temperature range of the $U_8O_{21\pm x} + U_3O_{8-z}$ diphasic domain. The non-stoichiometry range of U_3O_{8-z} is very narrow ($0.27264 < x(U) < 0.27284$), and the one of $U_8O_{21\pm x}$ a little larger ($0.27353 < x(U) < 0.27739$), and extends towards $UO_{2.61}$. Due to the lack of thermodynamic data, the non-stoichiometry range of these two compounds has been neglected in this work and we have considered only one stoichiometric compound U_3O_8 ($x(U) = 0.27273$).

5.2.2. Oxygen potentials

The $UO_{2\pm x}$ oxygen potential database is very important and relatively consistent. The data of Chapman and Meadows [68] in the temperature range 1273–1773 K, Chapman et al. [74] at 2200 and 3150 K, Une and Oguma [77] at 1573 and 1773 K, were found to be inconsistent with other values and thus discarded. No major inconsistency for the other authors was detected, and the data were used in the optimisation procedure with an adequate associated weight.

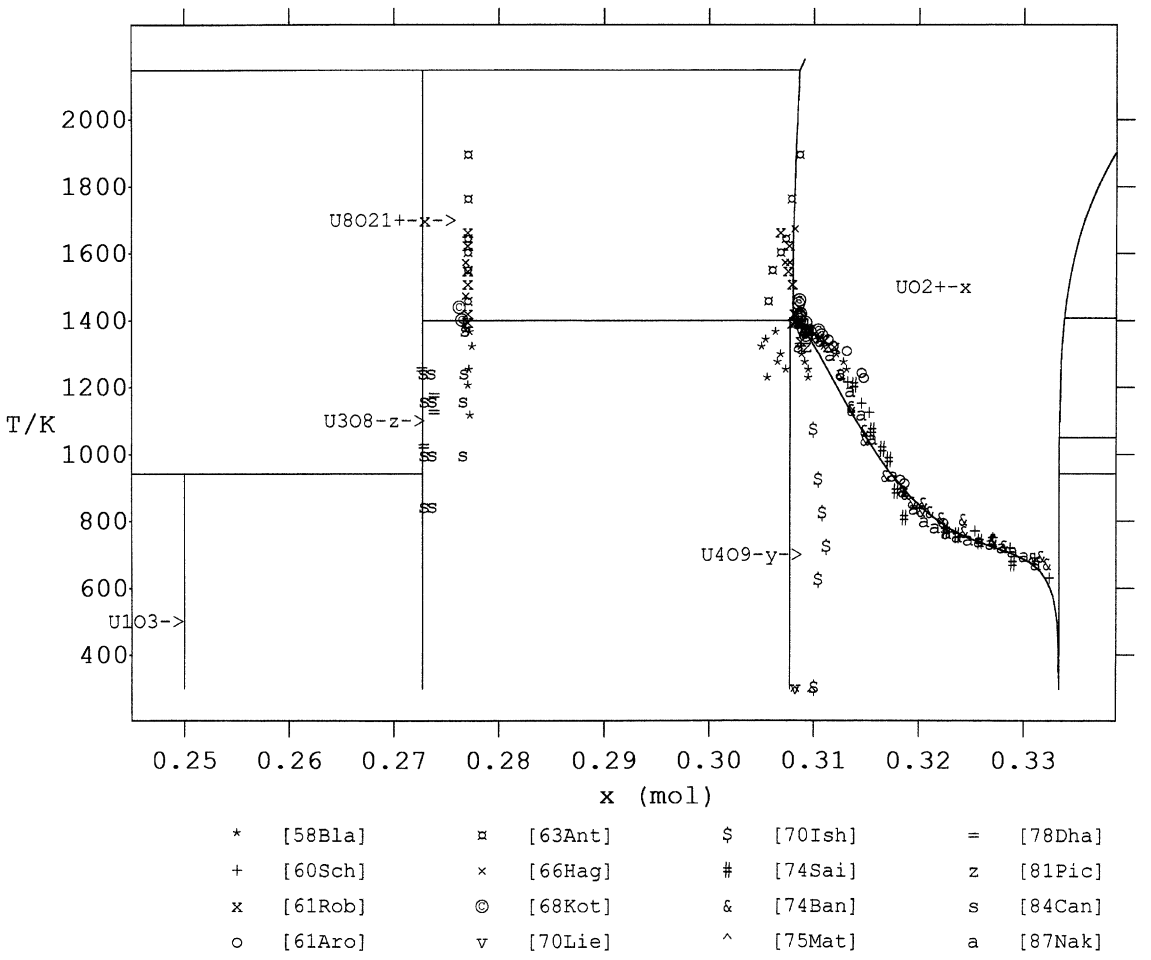

Fig. 8. Partial O–U phase diagram ($UO_{2\pm x}$ – O_2 region) compared to various experimental points.

5.3. Optimisation of solution interaction parameters

In the liquid phase, the reference substances are O_1^L, U_1^L, and $O_2U_1^L$. As O_2U_1 is very stable, the Gibbs energy of the liquid at the composition $x(U) = 0.333$ may be assimilated to the Gibbs energy of associate species $O_2U_1^L$. The O_1^L species are predominant in the hyper-stoichiometric domain, while the U_1^L are predominant in the hypo-stoichiometric domain. Thus, the interaction parameter between O_1^L and U_1^L may be neglected.

$$L[O_1, U_1]_1\langle L\rangle = 0.$$

The interaction parameter between O_1^L and $O_2U_1^L$ allows to describe the hyper-stoichiometric field, and thus $L[O_1, O_2U_1]_1\langle L\rangle$ is mainly optimised by using the Latta and Fryxell [13] data, in correlation with the UO_{2+x}, fcc_C1 solid solution.

The interaction parameter between $O_2U_1^L$ and U_1^L allows to describe the hypo-stoichiometric field, and thus $L[O_2U_1, U_1]_1\langle\langle L\rangle$ is mainly optimised by using the Martin and Edwards [5] and Latta and Fryxell [13] data, in correlation with the UO_{2-x}, fcc_C1 solid solution. This parameter is closely connected to the solubility of oxygen in L_2 and the shape of the miscibility gap $L_1 + L_2$.

In the $UO_{2\pm x}$, fcc_C1 phase, the reference substances are $O_3U_1^{fcc\_C1}$, $O_2U_1^{fcc\_C1}$, $O_1U_1^{fcc\_C1}$ and $U_1^{fcc\_C1}$. $O_2U_1^{fcc\_C1}$ is the stable reference. $U_1^{fcc\_C1}$ is the metastable reference substance concerning the hypo-stoichiometric field, $O_3U_1^{fcc\_C1}$ and $O_1U_1^{fcc\_C1}$ are the ones for the hyper-stoichiometric field. The Gibbs energy of these substances have been either arbitrarily estimated, either optimised; $O_1U_1^{fcc\_C1}$ is not influent and its Gibbs energy has been fixed to a high positive value.

The interaction parameters allowing to describe the hypo-stoichiometric field is $L[U_1^{(1)}]_1[O_1^{(2)}, Vo^{(2)}]_2[Vo^{(3)}]_1\langle UO_{2\pm x}$, fcc_C1$\rangle$. It is mainly optimised by using the solidus data below the monotectic temperature and the

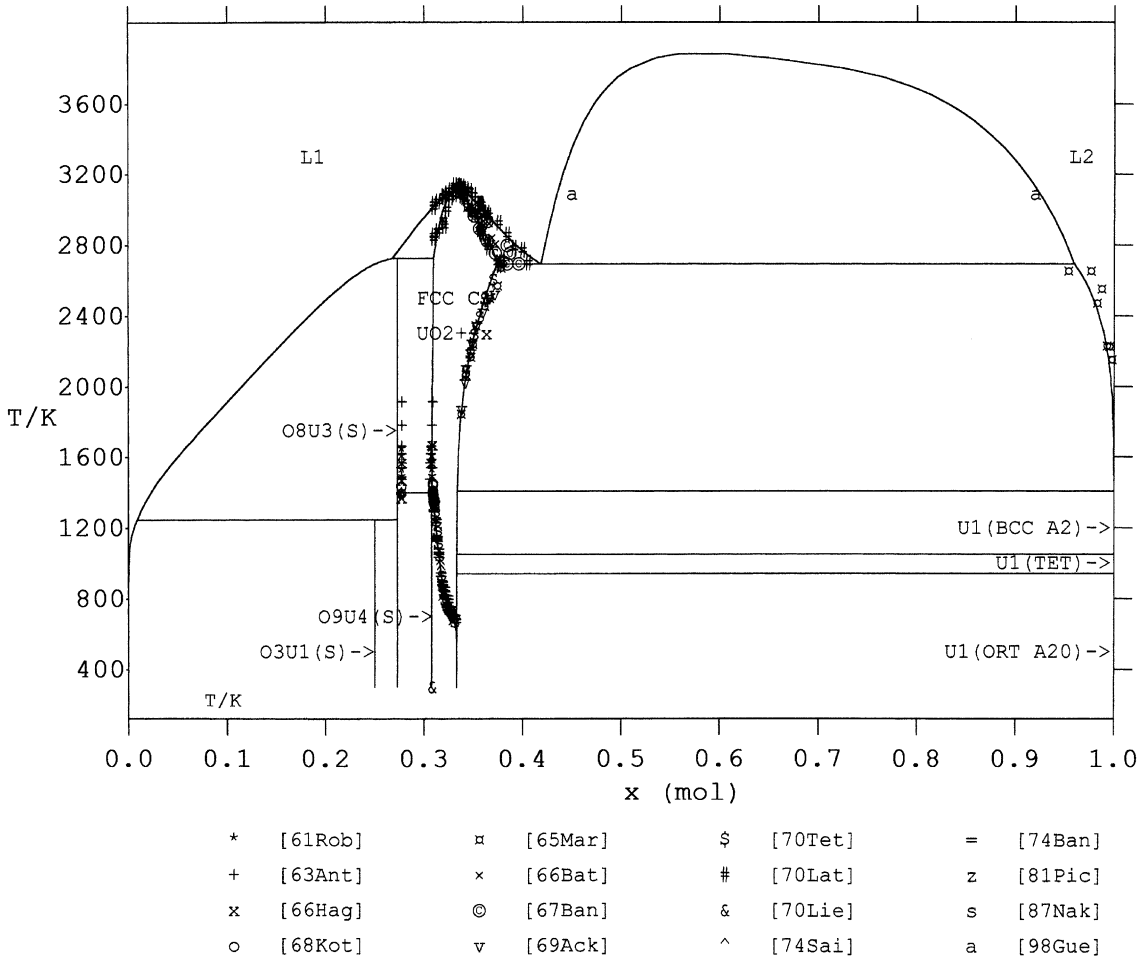

Fig. 9. Calculated O–U phase diagram without the gas phase compared to selected experimental points.

oxygen potentials. The other parameter $L[U_1^{(1)}]_1[Vo^{(2)}]_2[O_1^{(3)}, Vo^{(3)}]_1\langle fcc\_C1\rangle$ is not influent.

The interaction parameters allowing to describe the hyper-stoichiometric field is $L[U_1^{(1)}]_1[O_1^{(2)}]_2[O_1^{(3)}, Vo^{(3)}]_1\langle UO_{2\pm x}, fcc\_C1\rangle$. It is mainly optimised by using the solid–solid equilibria up to 2000 K and the oxygen potentials. The other parameter $L[U_1^{(1)}]_1[O_1^{(2)}, Vo^{(2)}]_2[O_1^{(3)}]_1\langle fcc\_C1\rangle$ is not influent.

6. Comparison of calculated phase diagram and oxygen potentials with experimental data

The phase diagram of the O–U system was calculated from the optimised Gibbs energy parameters for the condensed solution phases and the data taken from COACH [98] for the gas phase. It is presented with the quoted invariant reactions or special points on Fig. 5. The data of the gaseous species, i.e. $O_1(G)$, $O_2(G)$, $O_3(G)$, $O_1U_1(G)$, $O_2U_1(G)$, $O_3U_1(G)$ and $U_1(G)$, are reported in Table 14.

However, a complementary specific assessment work is still needed to improve the self-consistency of the O–U gaseous species thermodynamical properties. This work is going on and the results will be soon available.

Three main enlargements of the calculated phase diagram compared to the selected experimental information have been presented on Figs. 6–8. The $UO_{2\pm x}$ region for $0.24 < x(U) < 0.44$ and $1500 < T < 3300$ K is presented on Fig. 6.

The uranium-rich region for $0.9 < x(U) < 1$ and $1400 < T < 3300$ K is presented on Fig. 7.

The solid–solid equilibria ($0.2 < x(U) < 0.35$) and $300 < T < 2300$ K are presented in Fig. 8.

The partial phase diagram without the gas phase is presented in Fig. 9.

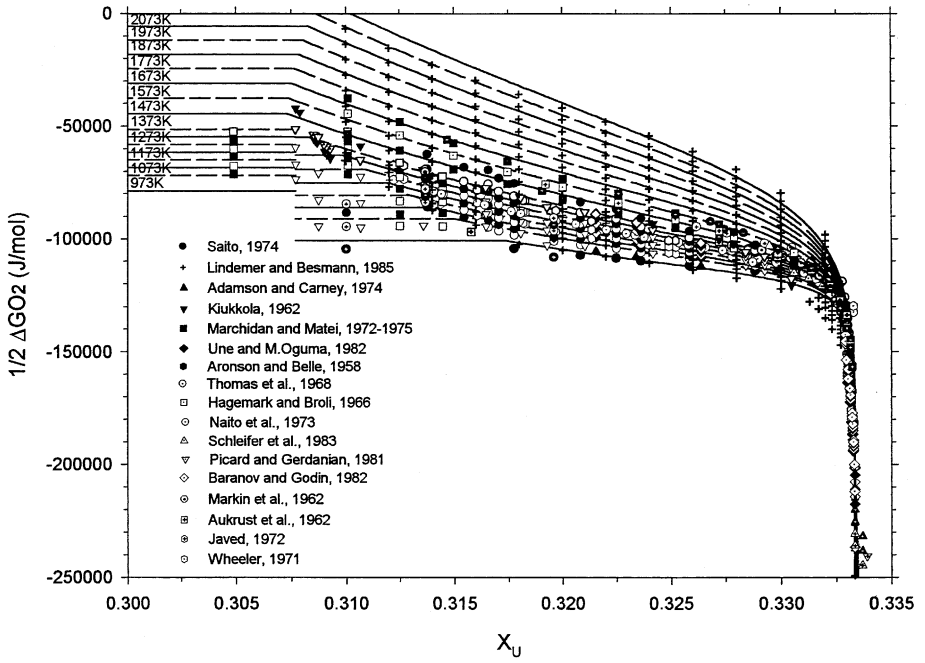

Fig. 10. Oxygen potentials of UO_{2+x} (hyper-stoichiometric region) compared to various experimental points in the temperature range 973–2073 K.

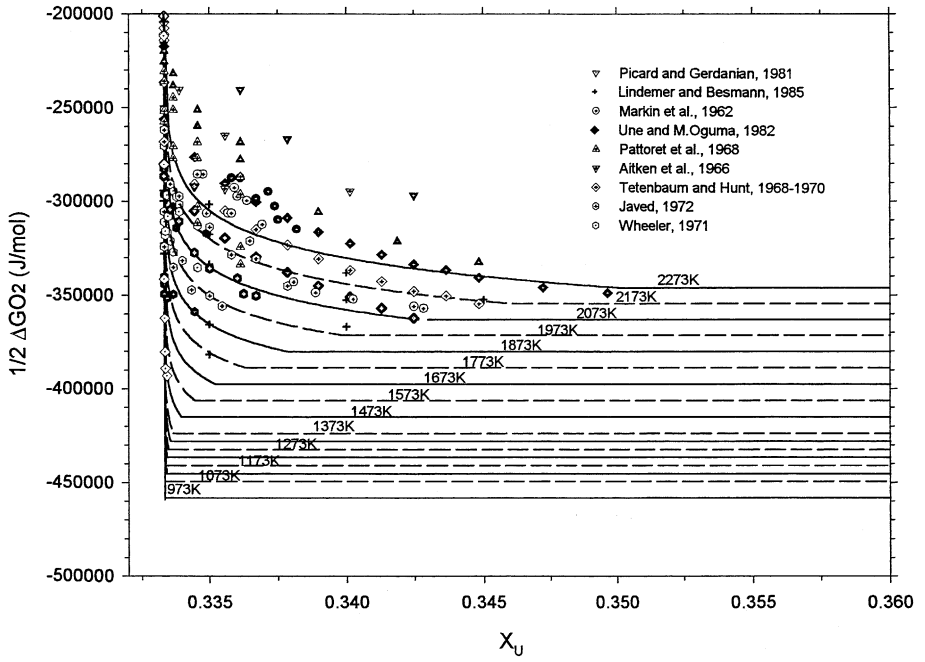

Fig. 11. Oxygen potentials of UO_{2-x} (hypo-stoichiometric region) compared to various experimental points in the temperature range 973–2273 K.

The calculated values from the assessment (phase diagram and thermodynamics) have been compared to experimental data in Tables 1–6, 9 and 10. The agreement between calculated and selected experimental

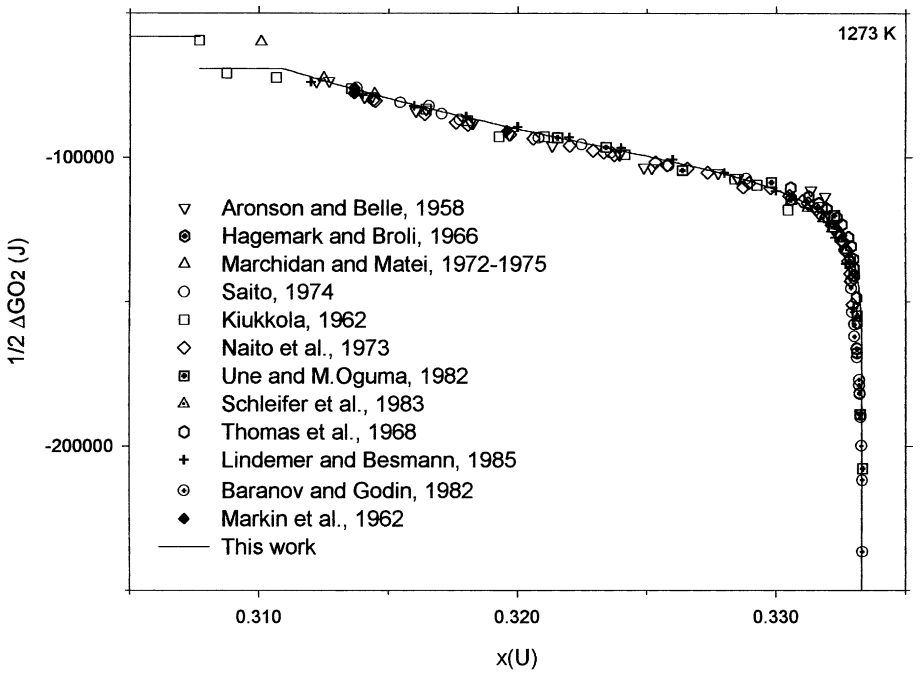

Fig. 12. Oxygen potentials of UO_{2+x} (hyper-stoichiometric region) compared to various experimental points at 1273 K.

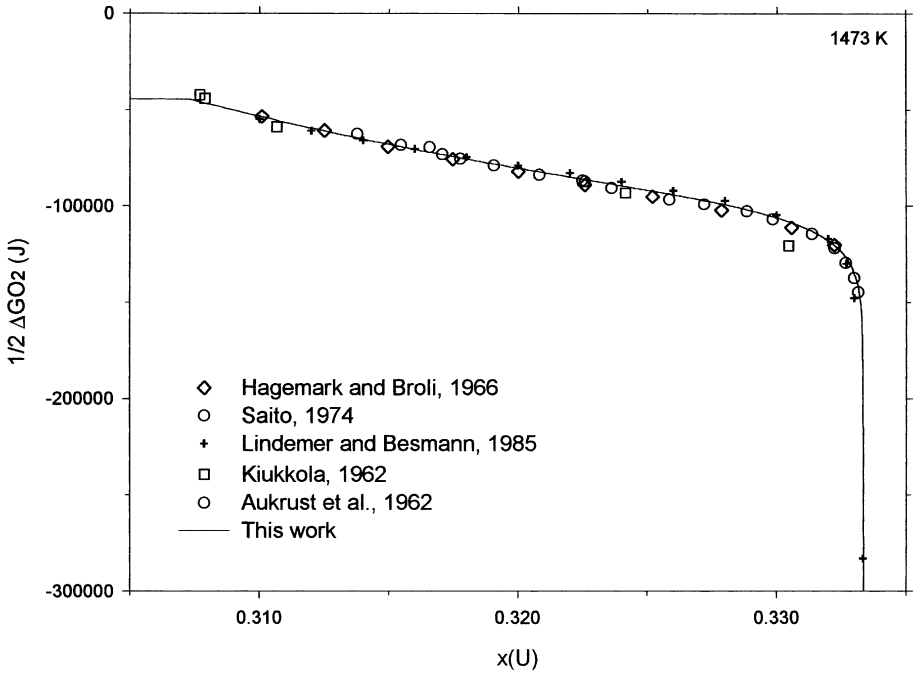

Fig. 13. Oxygen potentials of UO_{2+x} (hyper-stoichiometric region) compared to various experimental points at 1473 K.

values is quite satisfactory, whatever important differences were observed for the solubility of oxygen in liquid uranium. In Tables 7 and 8, the compounds were treated as stoichiometric.

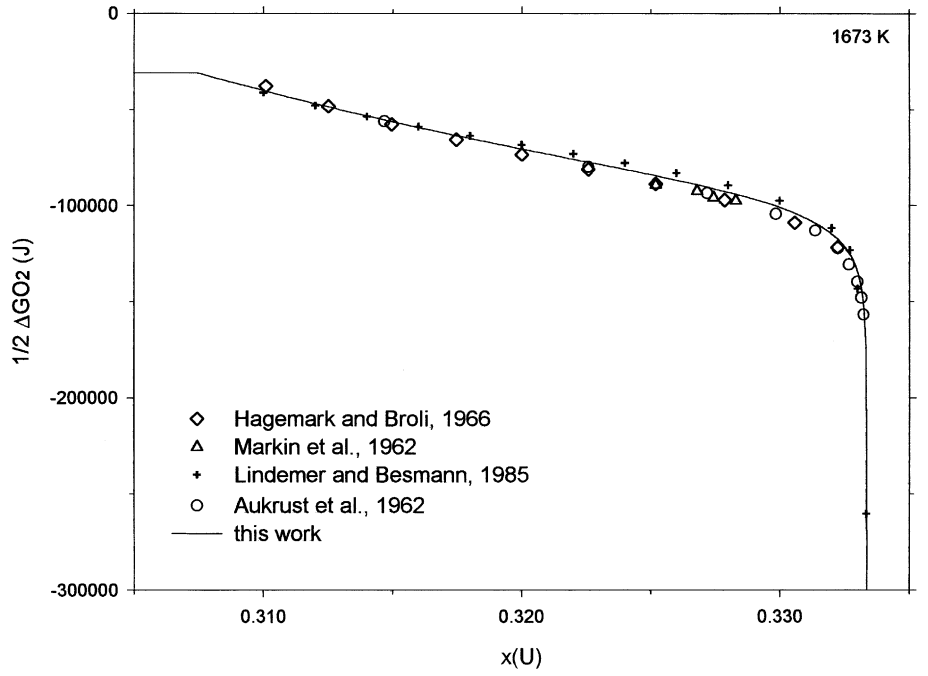

Fig. 14. Oxygen potentials of UO_{2+x} (hyper-stoichiometric region) compared to various experimental points at 1673 K.

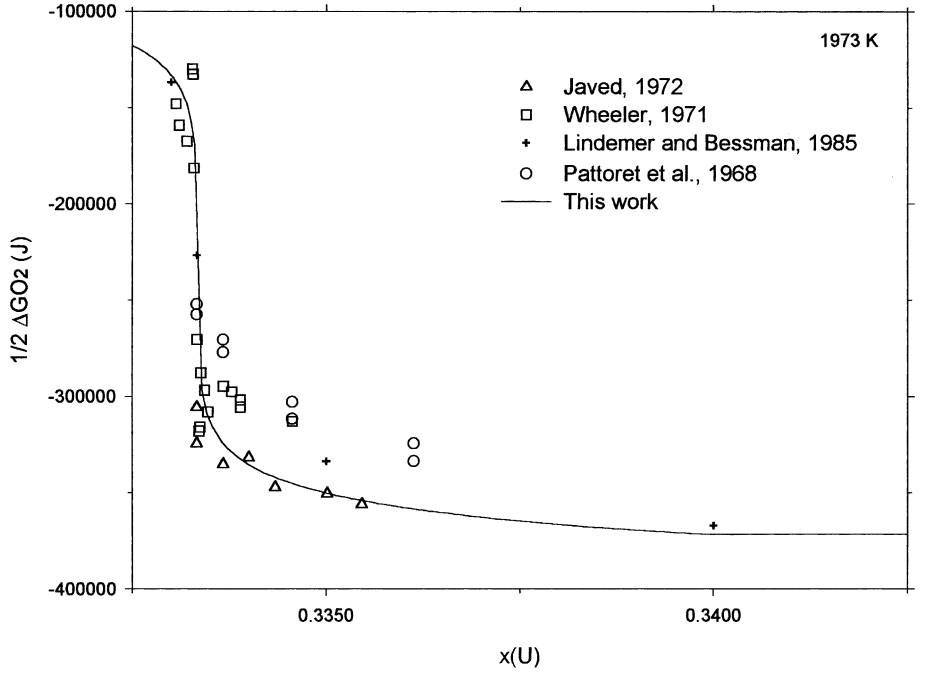

Fig. 15. Oxygen potentials of UO_{2-x} (hypo-stoichiometric region) compared to various experimental points at 1973 K

The oxygen potentials have been calculated in both hyper-stoichiometric and hypo-stoichiometric fields in the temperature range 773–2273 K and compared to available experimental data.

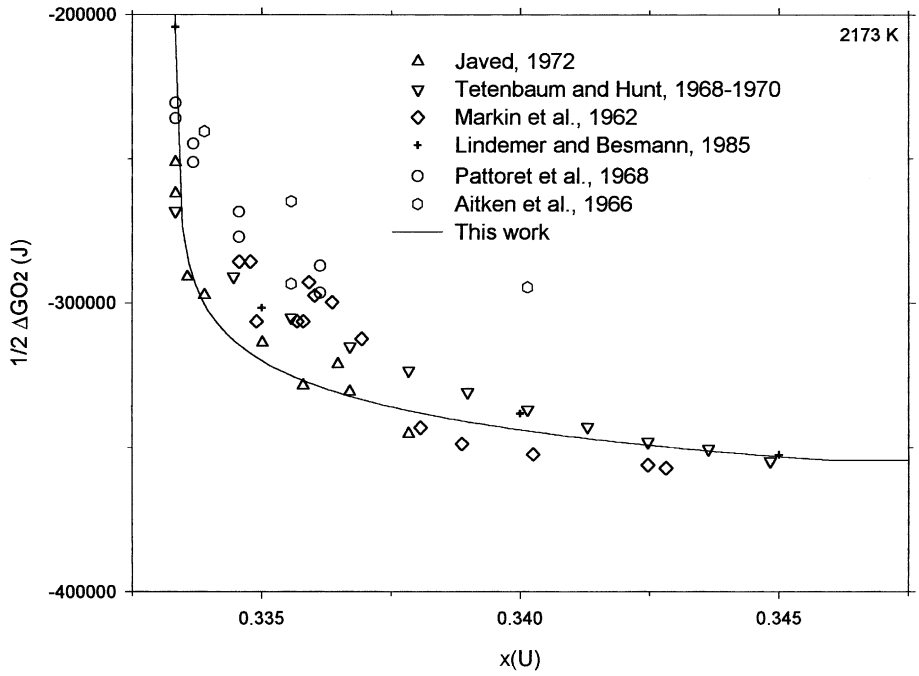

Fig. 16. Oxygen potentials of UO_{2-x} (hypo-stoichiometric region) compared to various experimental points at 2173 K.

Figs. 10 and 11 allow an overall comparison of the huge experimental oxygen potential database with the calculated one versus atomic composition and temperature. However, it is obvious that several figures are needed to precisely compare at each temperature the quality of the agreement with the corresponding experimental results.

To illustrate this purpose, the comparison has been detailed at 1273, 1473 and 1673 K in the hyper-stoichiometric field on Figs. 12–14, and at 1973 and 2173 K in the hypo-stoichiometric field in Figs. 15 and 16. The agreement in the hyper-stoichiometric field is quite satisfactory at all selected temperatures, while the model better fits the experimental values of Markin et al. [64] and Javed [66] than other ones in the hypo-stoichiometric field.

In summary, the overall comparison of the selected experimental data, as well as phase diagram as thermodynamic properties is quite satisfactory, even if improvements are always possible in some specific fields, due either to the selection of uncertainties of raw experimental data (often linked to the assessor analysis), or to the choice of the thermodynamic model and the number of optimised parameters.

7. Conclusion

In this work, we have presented an improved thermodynamic modelling of the very complex O–U binary system, based on the critical assessment of the very numerous experimental information, concerning both phase diagram and thermodynamic properties. We have modelled the liquid phase with a non-ideal associate model and the $UO_{2\pm x}$, fcc_C1 solid solution with a sublattice model, approximating the real structure of the phase. A set of optimised Gibbs energy parameters was produced: the thermodynamic properties of the stoichiometric substances and the $UO_{2\pm x}$, fcc_C1 solid solution have been reproduced as better as possible, especially the heat capacity and the oxygen potential experimental database; a very good self-consistency with the phase equilibria and oxygen potential data has been obtained, whatever a lack of accurate experimental data was still put in evidence for the solubility of oxygen in liquid uranium. The major aim of this work is to study much more complex systems involved in an hypothetical severe accident, in which urania may interact with many other materials (zircaloy, steel structures, control rods, concrete basemat) under the effect of reducing or oxidizing atmosphere at elevated temperatures. The non-ideal associate model used for the liquid phase in the present assessment is directly applicable. The use of a sublattice model, approximating the real structure, for the clearly ionic $UO_{2\pm x}$, fcc_C1 solid solution, may cause problems for dissolved fission products elements with different valency states, such as Ba, La or Sr. A different model, suitable for multi component applications, is being tested with the O–U–Zr ternary system.

Acknowledgements

This work was executed under the multi-partners project 'ENTHALPY' (European nuclear thermodynamic database validated and applicable in severe accident codes), co-financed by the European Commission under the 5th FrameWork Programme of the Euratom for Research and Training in the Field of Nuclear Energies (1998–2002). The authors wish to thank the partners: AEA-T, AEKI, CEA, EDF, Framatome–ANP, IPSN, SCK, Skoda, Thermodata, UCL, ULB, for valuable technical discussions.

References

[1] P.Y. Chevalier, E. Fischer, J. Nucl. Mater. 257 (1998) 213.
[2] E.M. Levin, C.R. Robbins, H.F. McMurdie, Phase diagrams for ceramists, Am. Ceram. Soc. (1964); 1969 Supplement, Figures 2067–4149 (Am. Ceram. Soc. 1969); E.M. Levin, H.F. McMurdie, 1975 Supplement, Figures 4150–4999 (Am. Ceram. Soc. 1975).
[3] R.S. Roth, T. Negas, L.P. Cook, Phase diagrams for ceramists, Figures 5000-5590, Am. Ceram. Soc., vol. 4, 1981.
[4] J.L. Bates, US At. Energy Comm. HW-81603 (1964) 2.15.
[5] A.E. Martin, R.K. Edwards, J. Phys. Chem. 69 (5) (1965) 1788;
R.K. Edwards, A.E. Martin, in: Thermodynamics of Nuclear Materials, vol. 2, IAEA, Vienna, 1966, p. 423.
[6] P.L. Blum, P. Guinet, H. Vaugoyeau, C.R. Acad. Sci. 257 (22) (1963) 3401.
[7] P. Guinet, H. Vaugoyeau, P.L. Blum, C.R. Acad. Sci. Série C 263 (1966) 17, rapport CEA-R3060, CENG, Section de Métallurgie, Nov. 1966.
[8] J.L. Bates, J. Am. Ceram. Soc. 49 (7) (1966) 395.
[9] M.J. Bannister, J. Nucl. Mater. 24 (1967) 340.
[10] R.J. Ackermann, E.G. Rauh, M.S. Chandrasekharaiah, J. Phys. Chem. 73 (4) (1969) 762.
[11] M. Tetenbaum, P.D. Hunt, J. Chem. Phys. 49 (11) (1968) 4739.
[12] M. Tetenbaum, P.D. Hunt, J. Nucl. Mater. 34 (1970) 86.
[13] R.E. Latta, R.E. Fryxell, J. Nucl. Mater. 35 (1970) 195.
[14] S.P. Garg, R.J. Ackermann, J. Nucl. Mater. 88 (1980) 309.
[15] R.J. Ackermann, E.G. Rauh, High Temp. Sci. 4 (1972) 496.
[16] S.P. Garg, R.J. Ackermann, Metall. Trans. 8A (1977) 239.
[17] C. Gueneau, V. Dauvois, P. Perodeaud, C. Gonella, O. Dugne, J. Nucl. Mater. 254 (1998) 158.
[18] P.E. Blackburn, J. Phys. Chem. 62 (8) (1958) 897.
[19] B.E. Schaner, J. Nucl. Mater. 2 (2) (1960) 110.
[20] L.E.J. Roberts, A.J. Walter, J. Inorg. Nucl. Chem. 22 (1961) 213.
[21] S. Aronson, J.E. Rulli, B.E. Schaner, J. Chem. Phys. 35 (4) (1961) 1382.
[22] A.M. Anthony, R. Kiyoura, T. Sata, J. Nucl. Mater. 10 (1) (1963) 8.
[23] K. Hagemark, M. Broli, J. Inorg. Nucl. Chem. 28 (1966) 2837.
[24] A. Kotlar, P. Gerdanian, M. Dodé, J. Chem. Phys. 65 (1968) 687.
[25] W. Van Lierde, J. Pelsmaekers, A. Lecocq-Robert, J. Nucl. Mater. 37 (1970) 276.
[26] T. Ishii, K. Naito, K. Oshima, Solid State Commun. 8 (1970) 677.
[27] K. Naito, T. Tsuji, T. Matsui, J. Nucl. Mater. 48 (1973) 58.
[28] M.J. Bannister, W.J. Buykx, J. Nucl. Mater. 55 (1974) 345.
[29] Y. Saito, J. Nucl. Mater. 51 (1974) 112.
[30] T. Matsui, K. Naito, J. Nucl. Mater. 56 (1975) 327.
[31] S.R. Dharwadkar, M.S. Chandrasekharaiah, M.D. Karkhanavala, J. Nucl. Mater. 71 (1978) 268.
[32] C. Picard, P. Gerdanian, J. Nucl. Mater. 99 (1981) 184.
[33] A. Caneiro, J.P. Abriata, J. Nucl. Mater. 126 (1984) 255.
[34] A. Nakamura, T. Fujino, J. Nucl. Mater. 149 (1987) 80.
[35] K. Kiukkola, Acta Chem. Scand. 16 (1962) 327.
[36] M.H. Rand, R.J. Ackermann, F. Gronvold, F.L. Oetting, A. Pattoret, Rev. Int. Hautes Tempé. Réfract. Fr. 15 (1978) 355.
[37] E.H.P. Cordfunke, R.J.M. Konings, G. Prins, P.E. Potter, M.H. Rand, Thermochemical data for reactor materials and fission products, Atomic Energy Research Establishment (AERE), Harwell, United Kingdom, European contract no. ETSN-005-NL, 1988.
[38] W.G. Mixter, Z. Anorg. Chem. 78 (1912) 221.
[39] W. Biltz, C. Fendius, Z. Anorg. Chem. 176 (1928) 49.
[40] E.J. Huber, C.E. Holley, E.H. Meierkord, J. Amer. Chem. Soc. 74 (1952) 3406.
[41] E.J. Huber, C.E. Holley, J. Chem. Thermodyn. 1 (1969) 267.
[42] M.M. Popov, M.I. Ivanov, Sov. J. At. Energy 2 (1957) 439.
[43] G.C. Fitzgibbon, D. Pavone, C.E. Holley Jr., J. Chem. Eng. Data 12 (1967) 122.
[44] M.H. Rand, O. Kubaschewski, The Thermodynamic Properties of Uranium Compounds, Interscience, New York, 1963.
[45] E.H.P. Cordfunke, P. Ailing, Trans. Faraday Soc. 61 (1965) 50.
[46] L.M. Vidavskii, N.J. Byakhova, E.A. Ippolitova, Zh. Neorg. Khim. 10 (1965) 1746.
[47] A. Duquesnoy, F. Marion, C.R. Acad. Sci. 258 (1964) 4550.
[48] A. Burdese, F. Abbattista, Ric. Sci. 28 (8) (1958) 1634.
[49] G.K. Johnson, P.A.G. O'Hare, J. Chem. Thermodyn. 10 (1978) 577.
[50] D.W. Osborne, E.F. Westrum, H.R. Lohr, J. Am. Chem. Soc. 79 (1957) 529.
[51] K. Gotoo, K. Naito, J. Phys. Chem. Solids 26 (1965) 1673.
[52] E.F. Westrum Jr., Y. Takahashi, J. Phys. Chem. 69 (1965) 3192.
[53] F. Gronvold, N.J. Kveseth, A. Sveen, J. Tichy, J. Chem. Thermodyn. 2 (1970) 665.
[54] A.C. Macleod, J. Chem. Thermodyn. 4 (1972) 699.
[55] H. Inaba, K. Naito, J. Nucl. Mater. 49 (1973/74) 181.
[56] M.M. Popov, G.L. Galchenko, M.D. Senin, Zurnal Neorgani Ceskov Himii 3 (1958) 1734.
[57] H.L. Girdhar, E.F. Westrum Jr., J. Chem. Eng. Data 13 (4) (1968) 531.
[58] K. Maglic, R. Herak, Rev. Int. Hautes Temp. Réfract. 7 (1970) 247.

[59] H. Inaba, H. Shimizu, K. Naito, J. Nucl. Mater. 64 (1977) 66.
[60] G.E. Moore, K.K. Kelley, J. Am. Chem. Soc. 69 (1947) 2105.
[61] W.N. Jones, J. Gordon, E.A. Long, J. Chem. Phys. 20 (4) (1952) 695.
[62] E.H.P. Cordfunke, E.F. Westrum Jr., Thermochim. Acta 124 (1988) 285.
[63] T.B. Lindemer, T.M. Besmann, J. Nucl. Mater. 130 (1985) 473.
[64] T.L. Markin, V.J. Wheeler, R.J. Bones, J. Inorg. Nucl. Chem. 30 (1968) 807.
[65] V.J. Wheeler, J. Nucl. Mater. 39 (1971) 315.
[66] N.A. Javed, J. Nucl. Mater. 43 (1972) 219.
[67] S. Aronson, J. Belle, J. Chem. Phys. 29 (1) (1958) 151.
[68] A.T. Chapman, R.E. Meadows, J. Amer. Ceram. Soc. 47 (12) (1964) 614.
[69] D.I. Marchidan, S. Matei, Rev. Roum. Chim. 17 (9) (1972) 1487.
[70] D.I. Marchidan, S. Matei-Tanasescu, Rev. Roum. Chim. 18 (10) (1973) 1681.
[71] D.I. Marchidan, S. Tanasescu, Rev. Roum. Chim. 19 (9) (1974) 1435.
[72] D.I. Marchidan, S. Tanasescu, Rev. Roum. Chim. 20 (11/12) (1975) 1365.
[73] K. Naito, N. Kamegashira, Adv. Nucl. Sci. Technol. 9 (1976) 99.
[74] A.T. Chapman, J. Brynestad, G.W. Clark, High Temp. – High Press. 12 (1980) 447.
[75] M.G. Adamson, R.F.A. Carney, J. Nucl. Mater. 54 (1974) 121.
[76] K. Une, M. Oguma, J. Nucl. Mater. 110 (1982) 215.
[77] K. Une, M. Oguma, J. Nucl. Mater. 115 (1983) 84.
[78] F. Schleifer, A. Naoumidis, H. Nickel, J. Nucl. Mater. 115 (1983) 143.
[79] C. Thomas, P. Gerdanian, M. Dodé, J. Chim. Phys. Phys. Chim. Biol. 65 (1968) 1349.
[80] V.J. Wheeler, I.G. Jones, J. Nucl. Mater. 42 (1972) 117.
[81] P. Gerdanian, M. Dodé, J. Chim. Phys. Phys. Chim. Biol. 62 (1965) 171.
[82] V.G. Baranov, Y.G. Godin, At. Energy, Engl. Transl. 51 (1982) 633.
[83] T.L. Markin, L.E.J. Roberts, A. Walter, in: Proc. Symp. Thermoyn. Nucl. Mater., IAEA, Vienna, 1962, p. 693.
[84] A. Pattoret, J. Drowart, S. Smoes, in: Proc. Symp. Thermoyn. Nucl. Mater., IAEA, Vienna, 1968, p. 613.
[85] E. Aukrust, T. Forland, K. Hagemark, in: Proc. Symp. Thermoyn. Nucl. Mater., IAEA, Vienna, 1962, p. 713.
[86] E.A. Aitken, H.C. Brassfield, R.E. Fryxell, in: Proc. Symp. Thermoyn. Nucl. Mater., vol. II, IAEA, Vienna, 1966, p. 435.
[87] B. Sundman, J. Agren, J. Phys. Chem. Solids 42 (1981) 297.
[88] F. Dolezalek, Z. Phys. Chem. 64 (1908) 727.
[89] I. Prigogine, R. Defay (Eds.), Thermodynamique Chimique, Dunod, Paris, 1950.
[90] O. Redlich, A.T. Kister, Ind. Eng. Chem. 40 (1948) 345.
[91] B.T.M. Willis, Nature (London) 197 (1963) 755.
[92] B.T.M. Willis, J. Phys. (Paris) 25 (1964) 431.
[93] T. Matsui, K. Naito, J. Nucl. Sci. Technol. 12 (1975) 250.
[94] The SGTE Casebook, Thermodynamics at Work, In: K. Hack (Ed.), Materials Modelling Series, Institute of Materials, London, 1996.
[95] A.T. Dinsdale, Calphad 15 (4) (1991) 317, updated in SGTE Database.
[96] H.L. Lukas, E.Th. Henig, B. Zimmermann, Calphad 1 (3) (1977) 225.
[97] A. Maurisi, C. Gueneau, P. Perodeaud, B. Schneider, O. Dugne, F. Valin, G. Bordier, Proc. Int. Conf. EUROMAT, October 1996..
[98] B. Cheynet, Computer software in chemical and extractive metallurgy, in: C. Bale, G. Irons (Eds.), Canadian Institute of Mining, Metallurgy and Petroleum, Montreal, Quebec, 1993, p. 33.